Jacob Eapen
Department of Nuclear Engineering,
North Carolina State University,
Raleigh, NC 27695
e-mail: jacob.eapen@ncsu.edu

Roberto Rusconi
School of Engineering and Applied Sciences,
Harvard University,
Cambridge, MA 02138

Roberto Piazza
Dipartimento di Ingegneria Nucleare,
Politecnico di Milano,
Milano 20133, Italy

Sidney Yip
Department of Nuclear Science and Engineering
and Department of Material Science and
Engineering,
Massachusetts Institute of Technology,
Cambridge, MA 02139

The Classical Nature of Thermal Conduction in Nanofluids

We show that a large set of nanofluid thermal conductivity data falls within the upper and lower Maxwell bounds for homogeneous systems. This indicates that the thermal conductivity of nanofluids is largely dependent on whether the nanoparticles stay dispersed in the base fluid, form large aggregates, or assume a percolating fractal configuration. The experimental data, which are strikingly analogous to those in most solid composites and liquid mixtures, provide strong evidence for the classical nature of thermal conduction in nanofluids. [DOI: 10.1115/1.4001304]

1 Introduction

A nanofluid is a colloid with complex thermo-chemical properties. Typical colloids, even in dilute concentrations, form aggregates that are dependent on the solution chemistry, surface charges, and thermal (Brownian) motion of the nanoparticles [1–3]. External fields such as gravity and temperature can support or disrupt the formation of aggregates. Thus in most experimentally tested nanofluids, there is a competition between the growth of fractal-like structures, coalescence into large clumps, sedimentation, and fragmentation [4]. The transport properties such as viscosity and thermal conductivity, in general, are sensitive to the geometrical configuration and the connectivity of the aggregated structures.

The study of thermal transport in colloidal dispersions is relatively recent. The thermophysical and thermal transport properties of magnetic colloids *(ferrofluids)* with nanoparticles as small as 4 nm were reported in the 1980s [5–7]. In the last decade, there has been a renewed interest with nonmagnetic metallic and oxide colloids. The early experiments on dilute nanofluids have shown a fascinating increase in the thermal conductivity [8–12] as well as other interesting effects of nanoparticle size and temperature [13,14]. The initial promise of nanofluids as an advanced, nano-engineered coolant, however, has been tempered in recent years by a lack of consensus on the thermal conduction mechanism. While several experiments with well-dispersed nanoparticles have shown modest conductivity enhancements consistent with the classical Maxwell theory for noninteracting spheres [15–24], more instances of larger enhancements have also been reported in recent years [25–45]. In a recent International Benchmark Exercise [46], different experimental techniques (such as transient hotwire and forced Rayleigh scattering) are shown to be comparable in accuracy and precision. Several outliers in the experimental data, however, highlight the difficulties of accurate thermal measurements in complex colloidal systems. Against this backdrop, it is essential to have a fundamental understanding of the heat conduction mechanism in nanofluids.

Contributed by the Heat Transfer Division of ASME for publication in the JOURNAL OF HEAT TRANSFER. Manuscript received December 30, 2008; final manuscript received December 18, 2009; published online July 23, 2010. Assoc. Editor: W. Q. Tao

The effective medium or mean-field theory of Maxwell [47,48] is most often used to analyze the thermal conductivity results of nanofluid experiments. For a nanofluid with *noninteracting* spherical nanoparticles, the theory predicts

$$\frac{\kappa}{\kappa_f} = \frac{1 + 2\beta\phi}{1 - \beta\phi} \tag{1}$$

where ϕ is the nanoparticle volume fraction, $\beta = (\kappa_p - \kappa_f)/(\kappa_p + 2\kappa_f)$, and $(\kappa_p - \kappa_f)$ is the difference between the thermal conductivities of the nanoparticle and the base fluid. If a finite temperature discontinuity exists at the nanoparticle-fluid interface, the Maxwell theory would still apply, provided that one makes the substitution $\kappa_f \rightarrow \kappa_f + \alpha\kappa_p$ (on the right-hand side), where $\alpha = 2R_b\kappa_f/d$, wherein R_b is the interfacial thermal resistance and d is the nanoparticle diameter [49,50].

The thermal conductivity enhancements beyond those predicted by Eq. (1) are often reported to be anomalous or unusual. In addition to larger thermal conductivities, experiments have also revealed other disagreements with the Maxwell theory. The thermal conductivity is observed to have an inverse dependence on the nanoparticle size [25,32,51,52] and a quasi-linear dependence on the temperature [14,36,53,54]. Interestingly, there appears to be a fundamental difference between the thermal conduction behavior of solid composites and nanofluids. In the former, smaller dispersed (or filler) particles, especially those in the nanometer size range, reduce the matrix thermal conductivity significantly. In some cases the thermal conductivity is reduced well-below that of the base medium [55] at all volume fractions, while in others, the enhancement is severely suppressed [56]. The solid composite behavior is easily explained through the interfacial thermal resistance R_b, which has an inverse dependence on the particle diameter [49,57,58]. Thus, decreasing the filler particle size will dramatically reduce the effective thermal conductivity of the solid composites and *vice versa*. For the case of nanofluids some of the experimental data indicate that the thermal conductivity increases with decreasing nanoparticle size—a behavior which is clearly at odds with the Maxwell theory [25,32,51,52]. Some experiments have also shown that the nanofluid thermal conductivity is not correlated in a simple manner to that of the nanoparticle as predicted by the Maxwell model [26,34]. A limiting behavior at higher volume fractions is also observed in nanofluids, which is

qualitatively different from that in solid composites. While the thermal conductivity displays a quadratic or power law behavior at higher volume fractions for solid composites [59,60], it is known to rise rapidly at lower volume fractions and then saturate at higher volume fractions for several nanofluids [26,28,34].

Several mechanisms have been recently proposed to account for the excess thermal conductivity and other departures from the Maxwell theory (such as temperature and size dependence). These include the Brownian motion of the nanoparticles [61,62], fluid convection at microscales [63–69], liquid layering at the particle-fluid interface [70–75], nanoparticle shape [46,76,77], cluster agglomeration [78,79], or a combination of the aforesaid mechanisms [80–85]. A disconcerting aspect of having several theories is compounded by the ability of each postulated mechanism to match (a subset) of the experimental data accurately.

In this paper, we start by asking an elementary question—Is there an anomalous thermal conduction behavior in nanofluids? First we show that the classical Maxwell theory has two limiting bounds, which correspond to two geometrical configurations of the nanoparticles. These limits are also formally known as the Hashin and Shtrikman (H-S) mean-field bounds for homogeneous composite media [48]. In the first configuration, the nanoparticles constitute the *dispersed* phase with the fluid medium acting as the continuous phase. Most investigations have thus far reported this lower limiting bound given by Eq. (1). In the second configuration, the nanoparticles can form the *continuous* phase with the base fluid constituting the dispersed phase. It is easy to visualize the second configuration for high volume fractions of nanoparticles, but for small volume fractions, the nanoparticles *will necessarily need to* form linear, fractal-like or percolating structures, separating large pockets of the fluid medium. In both configurations, the effective thermal conductivity is *maximally biased* toward the continuous phase. However, if the nanoparticles have a higher thermal conductivity in relation to the base fluid, the additional conduction paths in the second configuration will lead to an effective nanofluid thermal conductivity that is larger than what is given by the lower Maxwell limit (Eq. (1)).

Next, by analyzing a large body of data including those from our own experiments, we show that most of the reported thermal conductivity data are enveloped by the upper and lower Maxwell (H-S) mean-field bounds. This observation strongly indicates that the nanoparticles can exist in several configurations ranging from a well-dispersed mode to a linear chainlike arrangement in the colloidal state. Indeed, a number of electron microscopy experiments at low volume fractions support (but does not prove conclusively) the presence of both configurations. A comparison to the conduction behavior of solid-solid composites and liquid-liquid mixtures reveal that the Maxwell bounds, to a large extent, have a universal applicability. While this is recognized for solid-composites, it is not so well-known for liquid mixtures. We further show that the conduction behavior in binary solid composites differs from that of nanofluids in one important aspect, which is its susceptibility to interfacial thermal resistance for nanometer sized filler particles. The apparent anomalous behavior of nanofluids is thus shown to stem from the assumption of well-dispersed nanoparticles. If this restriction is removed the classical theoretical models can predict much higher thermal conductivities [86]. We further stress that the differences in aggregation structures, which arise from colloidal chemistry, thermodynamic conditions and external fields, have a profound influence on the nanofluid thermal conduction behavior. While a linear or fractal configuration provides additional conduction paths that promote the effective thermal conductivity, large aggregates or clumps (which are formed, for example, by sedimentation) are detrimental to thermal conductivity enhancements. In conclusion we show that the classical theory of thermal conduction is applicable to nanofluids – the phenomena being consistent with what is known for binary solid composites and liquid mixtures.

2 The Theoretical Framework for Thermal Conduction in Nanofluids

For a single component material, thermal conduction is described uniquely with the Fourier constitutive law $\dot{q}''=-\kappa\nabla T$, where κ is the thermal conductivity and T is the temperature. In a mixture heat can flow from multiple gradients in addition to the temperature gradient such as those resulting from concentrations and external fields. The theoretical framework for describing multicomponent transport is provided by the linear phenomenological theory, which postulates that the fluxes are linear homogeneous functions of the corresponding gradients. While an intrinsic thermal conductivity exists for the nanofluids, the measured thermal conductivity can include effects of diffusion, chemical reactions, and other external fields. Since diffusion, directly and indirectly, is considered to be a key mechanism for the nanofluid thermal conductivity in several new theories [61–69], the theoretical framework is elaborated here to make a quantitative assessment of diffusion and chemical reactions on nanofluid thermal conductivity. The formalism is well-known, and in this paper, it is adopted from de Groot and Mazur [87].

For a n component system, the linearity between the fluxes and gradients is expressed as

$$\mathbf{J} \equiv \mathbf{L}\hat{\mathbf{x}} = \sum_{k=1}^{n} L_{ik}\hat{X}_k \quad (i = 1,2, \ldots ,n) \tag{2}$$

where $\mathbf{J}$ and $\hat{\mathbf{x}}$ are the generalized flux and gradient vectors, respectively. $\mathbf{L}$ is a matrix containing the phenomenological coefficients. The cross coefficients L_{ik} and L_{ki} are equal, following Onsager's reciprocity hypothesis. The heat flux in a multicomponent system is not defined uniquely, and hence, the thermal conductivity. A commonly accepted definition follows from the second law of thermodynamics which is given by [87]

$$\mathbf{J}_q = \hat{\mathbf{J}}_q - \sum_{k=1}^{n} h^k \mathbf{J}^k \tag{3}$$

where $\hat{\mathbf{J}}_q$ is the heat flux, which is usually measured in an experiment, $\mathbf{J}_q$ is the reduced (or conductive) heat flux, $\mathbf{J}$ is the mass flux, and h is the partial specific enthalpy. The difference between $\mathbf{J}_q$ and $\hat{\mathbf{J}}_q$ represents the heat transfer due to diffusion. Typically, dilute nanofluid experiments are dominated by the gradients in temperature and concentration (to a lesser extent). For components (s,l), abbreviated for solid nanoparticles and base liquid, respectively, the phenomenological relationships reduce to the following form [87]:

$$\mathbf{J}_q = -L_{qq}\frac{\nabla T}{T^2} - L_{qs}\frac{1}{T}\nabla(\mu^s - \mu^l)_T \tag{4}$$

$$\mathbf{J}^s = -L_{sq}\frac{\nabla T}{T^2} - L_{ss}\frac{1}{T}\nabla(\mu^s - \mu^l)_T \tag{5}$$

where μ is the chemical potential. Note that for a binary nanofluid system, $\mathbf{J}^s=-\mathbf{J}^l$. In experiments, diffusion is associated with a concentration gradient (c) rather than the chemical potential. The above equations can be recast in terms of the experimental coefficients in the following form [87]

$$\mathbf{J}_q = -\kappa\nabla T - \rho_s\left(\frac{\partial\mu^s}{\partial c^s}\right)_{T,p} TD''\nabla c^s \tag{6}$$

$$\mathbf{J}^s = -\rho c^s c^l D_T \nabla T - \rho D^{sl}\nabla c^s \tag{7}$$

The phenomenological coefficients (L_{ik}) are related to the experimental coefficients in the following way:

$$\kappa = \frac{L_{qq}}{T^2} \tag{8}$$

$$D'' = \frac{L_{qs}}{\rho c^s c^l T^2} \tag{9}$$

$$D_T = \frac{L_{sq}}{\rho c^s c^l T^2} \tag{10}$$

$$D^{sl} = \frac{L_{ss}}{\rho c^l T}\left(\frac{\partial \mu^s}{\partial c^s}\right)_{T,p} \tag{11}$$

In Eqs. (6) and (7), D_T, D'', and D^{sl} stand for the thermal diffusion coefficient, the Dufour coefficient, and the mutual (binary) diffusion coefficient, respectively, while the density of the system is given by ρ. Thermal diffusion coefficient (D_T) accounts for the flow of matter with a temperature gradient, while the Dufour coefficient (D'') is a measure of the inverse effect, which is the flow of heat due to a concentration gradient. κ is the thermal conductivity of the nanofluid system, and it is clear that it is a native or intrinsic property of the nanofluid without any contribution from diffusion. The ratio of D_T to D^{sl} is defined as the Soret coefficient and is given by

$$s_T \equiv \frac{D_T}{D^{sl}} \tag{12}$$

In an experiment, measurements can be made before the diffusion transients begin ($\nabla c^s = 0$) or at steady-state conditions ($\mathbf{J}^s = \mathbf{J}^l = 0$). Therefore, multiple definitions for thermal conductivities can be defined as shown below for these limiting conditions [87].

$$\mathbf{J}_q = -\zeta \nabla T, \quad \hat{\mathbf{J}}_q = -\hat{\zeta} \nabla T \quad (\nabla c^s = 0) \tag{13}$$

$$\mathbf{J}_q = -\lambda \nabla T, \quad \hat{\mathbf{J}}_q = -\hat{\lambda} \nabla T \quad (\mathbf{J}^s = \mathbf{J}^l = 0) \tag{14}$$

The heat fluxes $\mathbf{J}_q$ and $\hat{\mathbf{J}}_q$ are associated with the thermal conductivities (ζ, λ) and $(\hat{\zeta}, \hat{\lambda})$, respectively. As mentioned before, the difference between these heat fluxes (Eq. (3)) is solely due to the heat carried by the diffusing nanoparticles. It can be shown that [87]

$$\zeta = \kappa$$

$$\hat{\zeta} = \kappa + D_T (h^s - h^l) \rho c^s c^l \tag{15}$$

$$\lambda = \kappa - \frac{(D_T)^2}{D^{sl}}\left(\frac{\partial \mu^s}{\partial c^s}\right)\rho (c^s)^2 c^l T$$

$$\hat{\lambda} = \lambda \tag{16}$$

where h denotes the partial specific enthalpy. Equations (15) and (16) correspond to the conditions $\nabla c^s = 0$ and $\mathbf{J}^s = \mathbf{J}^l = 0$, respectively. Thus for a measurement when the mass fluxes are zero, the effective thermal conductivity (λ) is always less than the intrinsic thermal conductivity (κ). At the beginning of the experiment when there are no concentration gradients, the effective thermal conductivity (ζ), as expected, is equal to that of the intrinsic value. A steady-state experiment corresponds to $\mathbf{J}^s = \mathbf{J}^l = 0$ while a transient hot wire measurement is closer to the condition $\nabla c^s = 0$. Equations (15) and (16) show the effect of diffusion on the thermal conductivity of a nanofluid, assuming that there are only two gradients, namely, temperature and concentration. The formalism can be extended to include other fields such as pressure gradient and external fields as long as the assumed linearity given in Eq. (2) is satisfied. In Sec. 3, we will give an estimate of the effective thermal conductivities with simple diffusion and with chemical reactions (since nanosized particles are known to be highly reactive).

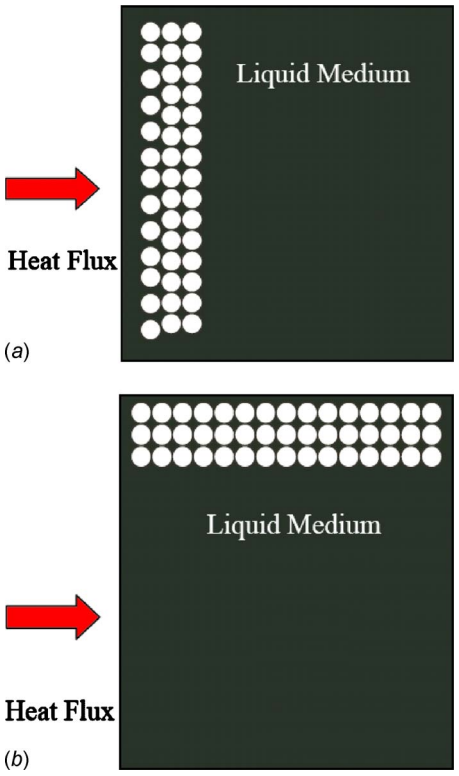

Fig. 1 A two-dimensional representation of (*a*) a series mode and (*b*) a parallel mode of thermal conduction in a binary nanofluid. Note that a typical nanofluid system is not inhomogeneous, as shown.

3 Postulated Mechanisms for Nanofluid Thermal Conduction

3.1 Classical Theories. The simplest and perhaps the most intuitive models correspond to the series and parallel modes of thermal conduction. In the former, the conducting paths, namely, those through the base fluid and the nanoparticles, are assumed to be in series, and in the latter, they are regarded to be in parallel (see Fig. 1). The effective thermal conductivities are given by [88,89]

$$\frac{1}{\kappa^{=}} = \frac{(1-\phi)}{\kappa_f} + \frac{\phi}{\kappa_p} \tag{17}$$

$$\kappa^{\parallel} = (1-\phi)\kappa_f + \phi \kappa_p \tag{18}$$

where $\kappa^{=}$ and $\kappa^{\parallel}$ are the series and parallel mode thermal conductivities, respectively.

In the dilute limit, as shown below, $\kappa^{=}/\kappa_f$ is a function of the volume fraction alone, while $\kappa^{\parallel}/\kappa_f$ is a function of the constituent thermal conductivities and volume fraction

$$\left(\frac{\kappa^{=}}{\kappa_f}\right)_{\phi \to 0} = 1 + \phi \tag{19}$$

$$\left(\frac{\kappa^{\parallel}}{\kappa_f}\right)_{\phi \to 0} = 1 + \phi \frac{\kappa_p}{\kappa_f} \tag{20}$$

From Eq. (20) it is clear that the enhancement in the parallel mode can be much larger than that in the series mode if $\kappa_p \gg \kappa_f$. As can be inferred from electron microscopy experiments, neither series nor parallel configuration is strictly applicable to most nanofluids even though the intertwined fibers allow nanotube suspensions to be approximated by the parallel mode. Since the parallel mode corresponds to a geometric configuration that allows the most ef-

ficient way of heat propagation, it represents the absolute upper limit for the effective thermal conductivity regardless of the phase of the constituents. For example, the experiments by Griesinger et al. have shown [90] an increase of 5000% in the thermal diffusivity of low density polyethylene when the polymer fiber fillers were configured *parallel* to the direction of the heat flow. Not surprisingly, numerous experiments have shown that the upper bound is rarely, if not ever, violated in binary solid composites or liquid mixtures.

The series and parallel bounds are not the narrowest that can be estimated with the classical approach. An analysis of the Maxwell's original work reveals that the theory predicts two bounds—*an upper and a lower bound*—also derived by Hashin and Shtrikman [48] using variational principles. In the first configuration, the nanoparticles constitute the dispersed phase with the fluid medium acting as the continuous phase. In the second configuration, the nanoparticles form the continuous phase with the base fluid constituting the dispersed phase. In both configurations, the effective thermal conductivity is maximally biased toward the continuous phase. The Maxwell (H-S) bounds for nanofluid thermal conductivity are given by [48,91]

$$\kappa_f\left(1+\frac{3\phi(\kappa_p-\kappa_f)}{3\kappa_f+(1+\phi)(\kappa_p-\kappa_f)}\right)\leq\kappa\leq\kappa_p\left(1-\frac{3(1-\phi)(\kappa_p-\kappa_f)}{3\kappa_p-\phi(\kappa_p-\kappa_f)}\right) \tag{21}$$

It is assumed that $\kappa_p>\kappa_f$ or otherwise, the upper and lower bounds would simply reverse. Notice that the lower Maxwell bound, which is identical to Eq. (1), is rigorously exact to the first order in the volume fraction. For a homogeneous system, the Maxwell theory predicts the above set of bounds, which is most restrictive on the basis of the volume fraction alone [48]. Any improvement on these bounds would require additional knowledge on the statistical variations in the dispersed medium. In addition to thermal conductivity, the above bounds are also applicable to other composite properties such as thermal diffusivity, electrical conductivity, and magnetic permeability.

While the lower bound has been extensively quoted in the nanofluid literature, the upper bound has not received much attention. For the lower Maxwell bound the nanoparticles are always well-dispersed, and therefore, the effective conductivity is biased toward the conduction paths through the surrounding fluid (see Fig. 2(*a*)). Theoretically, the upper bound should correspond to a configuration where continuous conduction paths emerge along the nanoparticles. It is straightforward to visualize this configuration for high volume fractions of nanoparticles, but for dilute nanofluids, the nanoparticles have to form a linear or chainlike configuration, separating large, noninteracting regions of base fluid. The correspondence between the mathematical idealization and physical realization is shown in Fig. 3.

If the nanoparticle thermal conductivity is higher than that of the base fluid, the effective thermal conductivity can be significantly enhanced by a chainlike or fractal configuration. All experimentally tested nanofluids have some form of aggregation, and thus, most of the enhancements beyond the Maxwell lower bound come from *limited* percolating effects (which can also manifest as nonspherical composite particles [46]). It is now easy to visualize that large nanoparticle clumps will *not* provide additional thermal conduction paths. Thus it is important to differentiate the difference between arbitrary coalescence (that occurs, for example, from settling of nanoparticles following ultrasonification), and stable, chainlike, percolating nanoparticle configurations.

With the two described configurations, it is easy to note that the lower Maxwell bound ($\kappa^{\mathrm{MX-}}$) lies closer to the series mode of conduction, while the upper bound ($\kappa^{\mathrm{MX+}}$) approaches the parallel mode. Also note that the variational formulation of Hashin and Shtrikman on Maxwell bounds does not place any restrictions on the volume fraction. If the configuration is neutral, i.e., neither favoring the series nor the parallel mode, then the effective thermal conductivity (κ^0) would lie between the lower and upper Maxwell bounds. This approach, attributed to Bruggeman and also sometimes known as the effective medium theory (EMT) [89], predicts the thermal conductivity in the implicit form given by

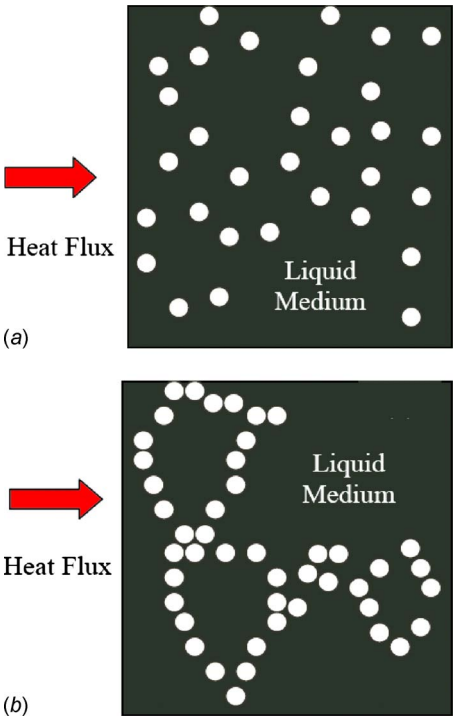

Fig. 2 A two-dimensional representation of the nanofluid configuration for the (*a*) lower and (*b*) upper Maxwell bounds

$$(1-\phi)\left(\frac{\kappa_f-\kappa}{\kappa_f+2\kappa}\right)+\phi\left(\frac{\kappa_p-\kappa}{\kappa_p+2\kappa}\right)=0 \tag{22}$$

In a nanofluid, the unbiased configuration would be a mix of well-dispersed nanoparticles and linear aggregation. All the classical models thus correspond to different configurations of the dispersed and continuous media. It can be shown for $\kappa_p>\kappa_f$

$$\kappa^{=}<\kappa^{\mathrm{MX-}}<\kappa^{0}<\kappa^{\mathrm{MX+}}<\kappa^{\parallel} \tag{23}$$

In the dilute limit with $\kappa_p>\kappa_f$, the lower Maxwell bound reduces to the well-known expression

$$\left(\frac{\kappa^{\mathrm{MX-}}}{\kappa_f}\right)_{\substack{\phi\to 0\\ \kappa_p\gg\kappa_f}}=1+3\phi \tag{24}$$

The recent model of Prasher et al. [78] assumes a linear chainlike cluster configuration for the nanoparticles, which is very similar to that for the upper Maxwell bound. The dilute limits are given by

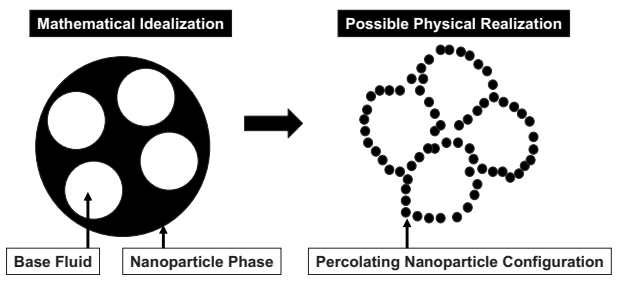

Fig. 3 Mathematical abstraction and physical realization for the Maxwell upper bound for dilute nanofluids

$$\left(\frac{\kappa^{\mathrm{MX+}}}{\kappa_f}\right)_{\phi\kappa_p/\kappa_f\to 0} = 1 + \frac{2\phi}{3}\left(\frac{\kappa_p}{\kappa_f}\right) \tag{25}$$

$$\left(\frac{\kappa^{\mathrm{Pr}}}{\kappa_f}\right)_{\phi\kappa_p/\kappa_f\to 0} = 1 + \frac{\phi}{3}\left(\frac{\kappa_p}{\kappa_f}\right) \tag{26}$$

where κ^{Pr} is the thermal conductivity predicted by the model of Prasher et al. [78]. The above limits and the parallel mode dilute limit [Eq. (20)] are identical except for the prefactor. It is thus evident that *linear*, *percolating* clustering effects can dramatically broaden the thermal conductivity range for the classical thermal conduction models. Interfacial thermal resistance has not been taken into account in any of these models yet, and if applicable, it is easily incorporated [49]. The interfacial resistance *always* reduces the effective thermal conductivity, and hence, the bounds presented here are the *highest* for the appropriate configurations [92].

In this paper, we will systematically explore the four classical bounds—series, lower and upper Maxwell, and parallel—for the reported data on nanofluids and make a critical comparison with those observed in solid-solid composites and liquid mixtures. Analogous behavior will imply classical conduction mechanisms in all three binary systems, while persistent or conspicuous violations of the upper Maxwell or parallel bounds will give credence to the anomalous thermal conduction behavior in nanofluids.

3.2 Interfacial Layer Models. The interfacial layer models can be considered under the classical models with the structure provided not by the clustering of nanoparticles but through an ordered fluid configuration around the nanoparticles [70–75]. As such, the predictions of interfacial layer models are enveloped by the classical bounds discussed before. Interestingly, the interfacial layer models are far more popular than those assuming nanoparticle clustering (even though experiments suggest otherwise) and thus, are treated as a separate mechanism in this paper.

We will analyze the current state of knowledge to make a reasonable assessment on the role of interfacial layers in nanofluids. The motivation for proposing this model stems from both theoretical and experiment evidences of ordered layering near a solid surface. For example, molecular dynamics simulations predict three ordered layers of water on the Pt (111) surface [93]. In the first layer, water molecules form icelike structures with the oxygen atoms bound to the Pt surface, while in the second and the third layers, water molecules that are hydrogen-bonded to the first and second layers, respectively, are observed. This ordering, even with a strong perturbation induced on the surface, persists over a distance of $O(1\ \mathrm{nm})$ from the Pt surface. Very similar behavior has been experimentally reported on a crystal-water interface [94]. Close to the interface, two layers of icelike structures strongly bonded to the crystal surface have been observed, followed by two diffuse layers with less pronounced lateral and perpendicular ordering. Direct experimental evidences are also available for thin layering with liquid squalane [95] and nonpolar liquids [96] adjacent to a solid surface.

In a recent molecular dynamics (MD) simulation it has been shown that atomic-sized clusters of the order of 10 atoms, which interact strongly with the host fluid, produce an amorphouslike fluid structure [97] near the cluster. This interfacial structure, which has a dimension of $O(1\ \mathrm{nm})$, provides a network of percolating conduction paths through the liquid medium [97]. The effective thermal conductivity is much higher than that of the lower Maxwell bound (50% enhancement for a volume fraction of 5%, approximately) but is enveloped by the upper Maxwell bound. However, when the clusters grow in size to hundreds of atoms, the percolation of interfacial structures gets impeded dramatically and the relatively large enhancements reduce to more modest values consistent with the lower Maxwell bound. These results are in agreement with an earlier molecular dynamics (MD) study [98], which showed no discernible increase in the interface thermal conductivity even while observing four ordered fluid layers near a surface. Similar results are also reported for water, which showed no dependence of the molecular orientation on the thermal conductivity [99].

A theoretical estimate for the interface thickness around a nanoparticle can be made from the Yan model [83], which is given by

$$h = \frac{1}{\sqrt{3}}\left(\frac{4M_f}{\rho_f N_a}\right)^{1/3} \tag{27}$$

where M_f and ρ_f are the molecular weight and density of the surrounding fluid medium around a nanocluster, respectively, and N_a is the Avogadro's number. For water-based nanofluids the Yan model gives an interfacial thickness of 0.284 nm, which is smaller than what is observed in the experiments or MD simulations, but agreeing on the order of magnitude.

Almost all the interfacial layer models, which have been proposed in the past, share the idea of a complex nanoparticle made of a bare nanoparticle and a postulated interfacial fluid nanolayer with an arbitrary thickness and thermal conductivity. Most models focus on nanoparticles that are of the order of 10 nm in size or smaller, and assume an interface thickness from 2 nm to 5 nm to provide evidence for a nanolayer-influenced thermal conduction mechanism. However, such assumptions are at variance with the theoretical and experimental evidences [94–96,100], which indicate that the interfacial layers are limited to a few molecular dimensions.

It is easy to show that an $O(1)$ nm layering is of no consequence to nanofluids that have been experimentally tested as the nanoparticle diameters (d) are mostly of the order of 10 nm and above [101]. Since the volume fraction scales as d^3, a 1 nm interfacial thickness for a 10 nm nanoparticle would correspond to a relative volume change of 10^{-3}, which is too small to account for any effect on the effective thermal conductivity. The experiments by Putnam et al. [20] show no unexpected increase in thermal conductivity for well-dispersed gold particles that are as small as 4 nm. These results are consistent with our experiments on dilute gold and platinum colloids (unpublished) and provide tangible evidence to the absence of ordered liquid structures that influence the thermal conductivity in nanofluids.

3.3 Brownian and Micro-convection Models. The recent Brownian and microconvection models attempt to rationalize the thermal conductivity enhancements as well as the temperature and size dependencies by postulating a diffusion dependent thermal conductivity, albeit, different from that given by Eqs. (15) and (16). The Brownian models [61,84] assume that that the nanofluid thermal conductivity is directly dependent on the self diffusion coefficient of the nanoparticle, which is given by the well-known Stokes–Einstein relationship $D = k_B T/(3\pi\mu d_p)$, where μ is the dynamic viscosity, d_p is the nanoparticle diameter, T is the absolute temperature, and k_B stands for the Boltzmann constant. While experimental trends for temperature and nanoparticle size are captured, this approach is criticized for several theoretical reasons, especially for the large mean free path of the liquid molecules with a magnitude of $O(1)$ cm [102,103]. In a Brownian dynamics (BD) simulation [62], the effect of diffusion is quantitatively estimated without resorting to explicit modeling. Many reported BD simulations, however, do not satisfy the momentum or energy conservation principles and hence, are incapable of predicting the thermal conductivity of colloidal systems. In classical BD simulations, the only quantity that is conserved is mass, and hence, the sole transport property that can be computed is the diffusion coefficient. When both momentum and energy conservation laws are enforced (in addition to mass conservation), BD (or dissipative particle dynamics) simulations have shown no tangible effect of Brownian motion on nanofluid thermal conductivity [104].

As discussed in Sec. 2, diffusion can enhance the thermal conductivity due to Soret effect and also through chemical reactions that can occur between the nanoparticles and the base fluid. In the

simple diffusion case, the enhancement in the thermal conductivity due to diffusion is $|\Delta\kappa| = D_T[(h^s - h^l)]\rho c^s c^l$ [87]. Typical values for nanofluid Soret coefficients are less than 0.1 K^{-1} [20,105,106]. This gives an upper bound on the thermal diffusion coefficient D_T of $O(10^{-10})$ $m^2\ s^{-1}\ K^{-1}$ with a diffusion coefficient D^{sl} of $O(10^{-11})$ m^2/s that corresponds to 10 nm sized nanoparticles. Note that the mutual and the self-diffusion coefficients are nearly the same for small volume fractions. Since the difference in the specific enthalpy (h) between the nanoparticles and the base fluid is typically of the order of 10^4 J/kg, it is relatively easy to see that the excess thermal conductivity $\Delta\kappa$ is several orders less than that of the base fluid. This conclusion is in agreement with several published reports [24,43,107,108].

At nanoscales, the nanoparticles can be exothermally reactive and diffusion accompanied by chemical reactions can also enhance the thermal conductivity [87]. If chemical equilibrium is reached quickly, the effective thermal conductivity can increase by [87]

$$\Delta\kappa = \frac{\rho_f D^{sl}(\Delta\hat{h})^2}{T\left(\frac{\partial\mu^s}{\partial c^s}\right)} \tag{28}$$

where $\Delta\hat{h}$ is the reaction heat (at constant temperature and pressure), which is of the order of the gradient in the chemical potential for the nanoparticles [87]. With a $\Delta\hat{h} = O(10^5)$ J/kg for reaction rates for nanoparticles in solutions (for example, the adsorption energy of water at the alumina surface is $\sim$140 kJ/mol [109]), $\Delta\kappa$ is again several orders less than that of the base fluid. Thus, there are sufficient theoretical reasons to believe that the diffusional motion of the nanoparticles does not *directly* influence the nanofluid thermal conductivity. Since thermodiffusion, mutual diffusion, and Brownian self-diffusion of the nanoparticles govern the aggregation processes, they will *indirectly* influence the transport properties of nanofluid systems [1,110–113]. Thus mechanisms of slow diffusional processes are extremely important to understand the effect of clustering on the nanofluid thermal conductivity [43,78,85,86].

In a related, but more intriguing hypothesis, the thermal conductivity is regarded to increase from convective transport of large volume of base fluid, which is dragged by diffusing nanoparticles [63–69]. In this "microconvection" picture, it is hypothesized that convection currents set up by the Brownian motion of the nanoparticles can enhance the heat transfer between the nanoparticles and the base fluid, and hence, the nanofluid thermal conductivity. In this paper, we will focus on two microconvection models that have received recognition in recent years. In the model of Jang and Choi [64,65], a new, but somewhat heuristic, heat transfer correlation is introduced to account for the randomly moving nanoparticles. It is given by

$$\mathrm{Nu} \equiv \frac{hd}{\kappa_f} = O(\mathrm{Re}^2\ \mathrm{Pr}^2) \tag{29}$$

The effective thermal conductivity can then be written as [65]

$$\frac{\kappa}{\kappa_f} = (1-\phi) + \frac{1}{(1+\hat{\alpha})}\left(\frac{\kappa_p}{\kappa_f}\right)\phi + C\left(\frac{d_f}{d_p}\right)\mathrm{Re}_d^2\ \mathrm{Pr}\phi \tag{30}$$

where $\hat{\alpha} \equiv R_b\kappa_p/d$ stands for a nondimensional interfacial thermal resistance, and Re_d and Pr denote the Reynolds number for the nanoparticle and the Prandlt number for the base fluid, respectively. With negligible microconvection and interfacial thermal resistance, the model of Jang and Choi coincides with the parallel mode of thermal conduction. A strong microconvection effect will, however, result in a thermal conductivity much higher than that of the parallel mode.

In the model of Prasher et al. [66,67], the traditional heat transfer correlation of flow over a sphere is adopted. Assuming that the Nusselt number on the scale of particle radius is $O(1)$, the Brownian motion of a single nanoparticle is regarded to increase the effective thermal conductivity of the base fluid by a factor of [1 + (1/4)Re Pr], A chief argument for microconvection hypotheses of Prasher et al. (and Jang and Choi) comes from the presumed presence of interfacial thermal resistance for the nanoparticles. Indeed, for nanosized filler particles in a solid composite, the effect of interfacial resistance can be very pronounced. Thus to account for the interfacial thermal resistance and the mixing of convection currents from multiple nanoparticles, the thermal conductivity of the nanofluid is fitted to experimental data using the expression [66]

$$\frac{\kappa}{\kappa_f} = (1 + A\ \mathrm{Re}^{\gamma}\ \mathrm{Pr}^{0.333}\ \phi)\left(\frac{1+2\beta\phi}{1-\beta\phi}\right) \tag{31}$$

where γ is a system-specific exponent, which, for aqueous suspensions, is found to have an optimal value of 2.5, and A is a constant attaining values as large as 4×10^4. For negligible microconvection effects and interfacial thermal resistance, the model of Prasher et al. reduces to the Maxwell expression for well-dispersed nanoparticles (lower bound).

We will now examine the characteristics of the microconvection models in more details. The hypothesized microconvection effects appear through $\mathrm{Re}_d = Vd/\nu$, where V and ν are the convection velocity and the base fluid kinematic viscosity, respectively. In both the microconvection models, the convection velocities are represented by a "Brownian velocity" to account for the rapidly oscillating nature of nanoparticle motion. In the Jang and Choi model, V is given by [64]

$$V = \frac{D^{ss}}{l_f} = \frac{k_B T}{3\pi\mu d_p l_f} \tag{32}$$

where l_f is the mean-free path of a base fluid molecule and D^{ss} is the self-diffusion coefficient of the nanoparticle. As noted by the authors, it is not clear whether the above ratio actually represents a random velocity of the nanoparticle. In the model of Prasher et al. (as also in Ref. [63]), the conventional thermal velocity of the nanoparticle is taken as the convection velocity, which is given by [66]

$$V = \sqrt{\frac{3k_B T}{m}} = \sqrt{\frac{18k_B T}{\pi\rho {d_p}^3}} \tag{33}$$

where m and ρ are the mass and density of the nanoparticle, respectively. Interestingly, a different form is adopted in the Patel microconvection model [69], which is given by

$$V = \frac{2k_B T}{\pi\mu {d_p}^2} \tag{34}$$

The latitude in choosing several forms, and therefore, differing physical characteristics, stems from the nonrigorous concept of a Brownian velocity. In the formal theory of Langevin dynamics, a fluctuating thermal velocity is uniquely defined, while velocities constructed based on diffusion characteristics are not.

Two peculiar consequences of Eq. (33) are that, for a given base fluid, temperature, and nanoparticle size, the enhancement in the thermal conductivity increases with decreasing nanoparticle density ρ, and for nanoparticles with low density, the thermal conductivity can be largely positive even if $\kappa_p < \kappa_f$. In our recent work [91], we had explicitly tested this prediction with the transient hot-wire (THW) technique on nanofluids with silica and MFA (a copolymer of tetrafluoroethylene and perfluoro-methylvinylether) nanoparticles that are lighter than the commonly tested alumina and copper oxide nanoparticles. We will report the main results briefly. Equation (1) predicts κ_p/κ_f to be a universal function of $\beta\phi$ while the microconvection model does not. In Fig. 4, we plot two sets of data for Ludox and MFA as a function of $\beta\phi$ along with the reported experimental data in the literature for alumina and copper oxide, which have higher densities, as previously men-

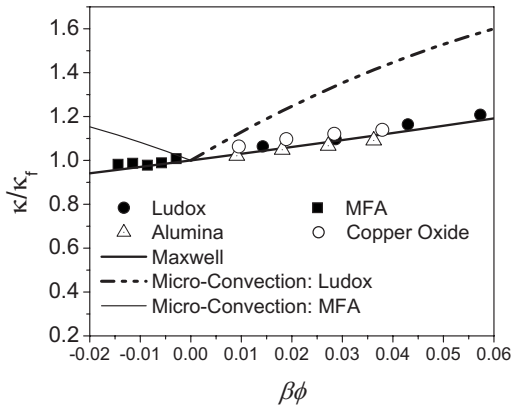

Fig. 4 THW data for Ludox ($\rho\sim2200$ kg/m^3, $d=32$ nm), MFA ($\rho\sim2140$ kg/m^3, $d=44$ nm), Al_2O_3 ($\rho\sim4000$ kg/m^3, $d=38$ nm), and CuO ($\rho\sim6300$ kg/m^3, $d=29$ nm) suspensions, plotted as a function of $\beta\phi$. The deviation of microconvection model from the Maxwell lower bound for Al_2O_3 and CuO are comparable to the experimental uncertainty.

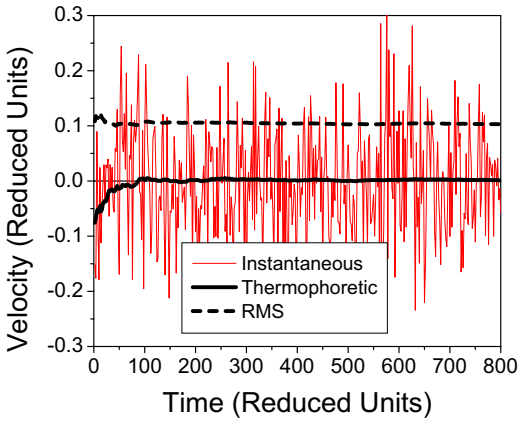

Fig. 5 Typical instantaneous and thermophoretic drift velocities in the *z*-direction of a 100 atom solid nanoparticle in a generic LJ fluid with NEMD simulations [97]. The rms velocity of the nanoparticle (0.1) is very close to $V=\sqrt{k_BT/m}$.

tioned. Quite remarkably, all the experimental data collapse on to a single line predicted by the Maxwell theory for noninteracting spheres (lower bound) without any interfacial thermal resistance and regardless of the nanoparticle density (or size). However, assuming microconvection contributions lead to system-dependent predictions, which are strongly conflicting with the experiments.

We have attributed the overprediction of the microconvection model from ascribing the nanoparticle thermal velocities as the convection velocities in place of the significantly lower thermophoretic drift velocities [91]. As explained in Sec. 2, an introduction of a thermal gradient, nonequilibrium coupling between mass and heat transport takes place due to the Soret effect. Thus, a colloidal particle acquires a thermophoretic drift velocity given by $u_T=D_T\nabla T$ [106]. For nanoparticles, which are sufficiently larger than the molecular dimensions, the small Knudsen number makes the no-slip interface conditions a reasonable approximation [114]. Thus in typical thermal conduction experiments, the microconvection velocities can only be of the order of the thermophoretic velocities.

Compared with the magnitude of the strongly fluctuating thermal speed, the thermophoretic velocities are insignificant in a nanofluid as they are characteristic of the collective motion of fluid motion around several diffusing nanoparticles. Our optical thermal lensing measurements have yielded a value of $D_T\sim10^{-12}$ m^2 s^{-1} K^{-1} for both Ludox and MFA colloids, which with typical THW temperature gradients correspond to thermophoretic velocities as low as 1 nm/s, while the assumed convection velocities in the models of Prasher et al. and Jang and Choi are $O(1)$ m/s and $O(0.1)$ m/s, respectively. Theoretical estimates of the colloidal drift speeds are also in the range of $O(10^{-8})$ m/s [105], which is consistent with our experimental values. To show that the thermophoretic velocities are insignificant even for very small nanoparticles, we have performed nonequilibrium molecular dynamics (NEMD) simulations on a model system. The details of the simulation method are given in Ref. [97]. Figure 5 shows the relative magnitudes of the typical instantaneous nanoparticle velocity and the corresponding thermophoretic drift velocity. At steady state the magnitude of the thermophoretic drift velocity is two orders smaller than that of the root-mean-square (rms) value.

The fact that the particle thermal velocity is not the relevant velocity scale for heat transport is seen from a simple argument. One should indeed compare the distance a particle moves within a Brownian relaxation time $\tau=m/f$, where f is the particle friction coefficient corresponding to the typical spatial scales of the macroscopic thermal gradients. For particles in the few tens of the nanometer size range, $\tau\sim O(10^{-10})$ s—a time scale which corresponds to a particle displacement of a few thousands of its diameter. The relaxation time τ, which also sets the time decay of correlations between the particle momentum and energy density flux in the liquid [115], is negligible on the time scales probed by THW measurements. The difference of several orders of magnitude in the convection velocities thus precludes a significant contribution to the thermal conductivity from *any* conceivable microconvection mechanism.

4 Classical Bounds

In Sec. 3, we have provided experimental and theoretical evidences to show that the interfacial layers, Brownian motion and microconvection do not influence the thermal conductivity of the commonly tested nanofluids. In this section, we show that the classical theories are capable of explaining the rather large thermal conductivity enhancements reported so far. In addition, we also show that nanofluid thermal conduction behavior is strikingly similar to that observed in solid-composites and liquid mixtures by examining the theoretical bounds discussed in Sec. 3. However, we find that the interfacial thermal resistance, which is inferred from a large body of experimental data, is negligible for most nanofluids, but can become significant for solid-composites.

4.1 Classical Bounds for Solid Composites. We will start by discussing the classical bounds for solid-composites. As discussed before the upper and lower Maxwell bounds (H-S) are the narrowest bounds that can be constructed on the basis of volume fraction alone. The Maxwell bounds, in turn, are enveloped by those from the series and parallel mode of conduction. The spread of the bounds depend on the relative thermal conductivities of the media. Most experiments with binary solid composites have a large difference in the thermal conductivities, and thus a relatively large spread ranging several orders can be expected.

In Fig. 6, we have delineated the thermal conductivity enhancements for a large number of solid composite materials. The classical bounds are calculated based on the thermal conductivity data given in the Appendix. At larger volume fractions ($\phi>10\%$), the experimental data largely lie between the lower and upper Maxwell bounds. At lower volume fractions ($\phi\leq10\%$), the thermal conductivity falls below the lower Maxwell bound for a few composites, and for polyethylene–Cu, polyethylene–Zn, and ZnS–diamond, it becomes lower than the series mode prediction. Additionally, as the size increases, the thermal conductivity increases significantly (polypropylene–Al, polyvinylidene–AlN, and ZnS–diamond). All these observations can be reconciled within the

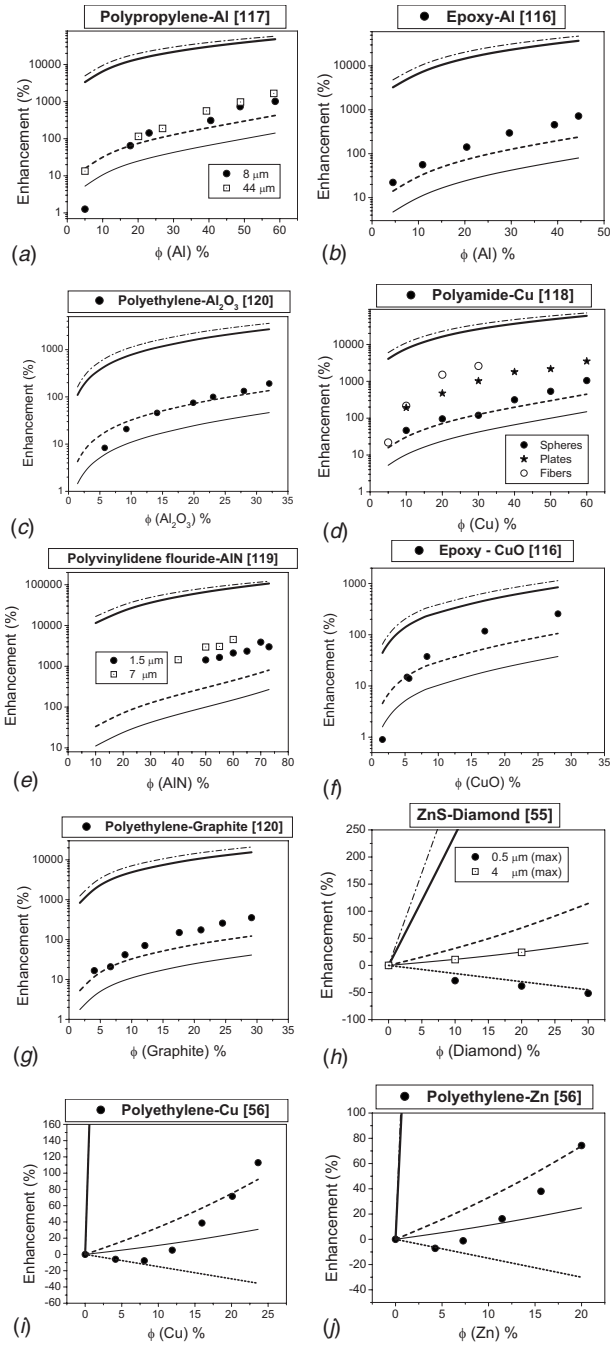

Fig. 6 Classical bounds for thermal conductivity in solid composites. The thin solid and thin dashed-dotted lines denote enhancements in thermal conductivity (or diffusivity) with the series and parallel modes, respectively. The upper Maxwell bound is delineated by the thick solid line while the lower Maxwell bound is given by the thick dashed line. The experimental data are represented by symbols. A fifth bound given by $(1-3\phi/2)$ for polyethylene–Cu, polyethylene–Zn, and ZnS–diamond (dotted line) denotes the limiting condition $\alpha\to\infty$. Table 1 in the Appendix gives the numerical values used in the calculation of classical bounds. Experimental data are taken from [55], [56], and [116–120].

framework of classical theories. The nondimensional interfacial resistance parameter $\alpha\equiv 2R_b\kappa_f/d$ determines the temperature discontinuity at the filler particle (p)-base medium (m) interface. In the limit $\kappa_p \gg \kappa_m$, the Maxwell lower bound can be expressed as

$$\frac{\kappa}{\kappa_m}=\frac{(1+2\alpha)+2\phi(1-\alpha)}{(1+2\alpha)-\phi(1-\alpha)} \tag{35}$$

Since α increases for decreasing filler particle size the effective thermal conductivity also decreases, which is consistent with the experimental data on polypropylene–Al, ZnS–diamond, and polyvinylidene fluoride–AlN. In the limit of $\alpha\to\infty$, κ/κ_m reduces to $(1-3\phi/2)$. Thus, the effective thermal conductivity can become smaller than that of the base medium for all volume fractions, as attested by the data for ZnS–diamond with 0.5 μm particles. Furthermore, the data for polyethylene–Cu and polyethylene–Zn are also bounded by $(1-3\phi/2)$.

Well-dispersed large spheres largely follow the lower Maxwell limit except at higher volume fractions. As the volume fraction increases the filler particles tend to form chainlike configurations, which promote a better heat transfer, and hence, the thermal conductivity. This formation of interconnected or percolating filler particles explains the rapid nonlinear increases in the thermal conductivity at higher volume fractions (see polyethylene–Cu and polyethylene–Zn in linear scale). The filler materials in the form of fibers, as observed with polyamide–Cu, are also very efficient for heat transfer. In a more dramatic observation, polyethylene polymer, a material having a low κ of 1 W/m K, increases its thermal conductivity to 50 W/m K, close to that of steel, when the polymer chain orientation is made parallel to the heat flow [90]. We emphasize here that the upper Maxwell bound is never violated for any of the experimental data.

4.2 Classical Bounds for Liquid Mixtures. Unlike those in solid composites, the classical bounds in liquid mixtures are not well-recognized. In the Sutherland–Wassiljewa theory, the thermal conductivity of a liquid mixture is given by [121]

$$\kappa=\kappa_1\left(\frac{n_1}{n_1+A_{12}n_2}\right)+\kappa_2\left(\frac{n_2}{n_2+A_{21}n_1}\right) \tag{36}$$

where n denotes the mole fraction and 1 and 2 stand for the two components. The coefficient A, also known as the Wassiljewa coefficient, is given by the following semi-empirical form [122]:

$$A_{ij}=\frac{1}{4}\left[1+\left(\frac{\kappa_i}{\kappa_j}\right)^{1/2}\left(\frac{M_j}{M_i}\right)^{1/4}\right]^2\left[\frac{2M_j}{M_i+M_j}\right]^{1/2} \tag{37}$$

where M denotes the molecular weight. We can observe that for equimolar liquids and $A_{12}=A_{21}=1$, Eq. (36) is identical to that of the parallel mode of thermal conduction.

In Fig. 7 we show the four bounds for a few representative liquid mixtures along with the unbiased or Bruggeman effective medium estimate given by Eq. (22). Most the data are nestled between the upper and lower Maxwell bounds. Due to a smaller difference between the thermal conductivities of the two media, the bounds are relatively narrower. While liquids, in general, do not have identifiable structures, networked bonds such as in water can facilitate liquid molecules to form loosely formed dynamic structures with characteristics of both interconnected chains and isolated blocks of molecules. Such an arrangement will be consistent with that of the unbiased Bruggeman effective medium model. Indeed, we find that most of the data on liquid mixtures are best predicted by the Brugemman model.

4.3 Classical Bounds for Nanofluids. For both solid composites with negligible interfacial thermal resistance and liquid mixtures, Maxwell bounds are respected to a large degree. However, these bounds have not been tested so far for nanofluids.

The first test of the theoretical bounds is conducted by analyzing the test data of magnetic (Fe_3O_4) nanofluids [39,45] (or ferrofluids). Strong magnetic fields induce magnetic nanoparticles to form chainlike configurations, and when the magnetic field is applied parallel to the heat flux (or ∇T), a strong thermal conductivity enhancement is observed, as shown in Fig. 8. An increasing magnetic field correlates to an enhanced chainlike formation of

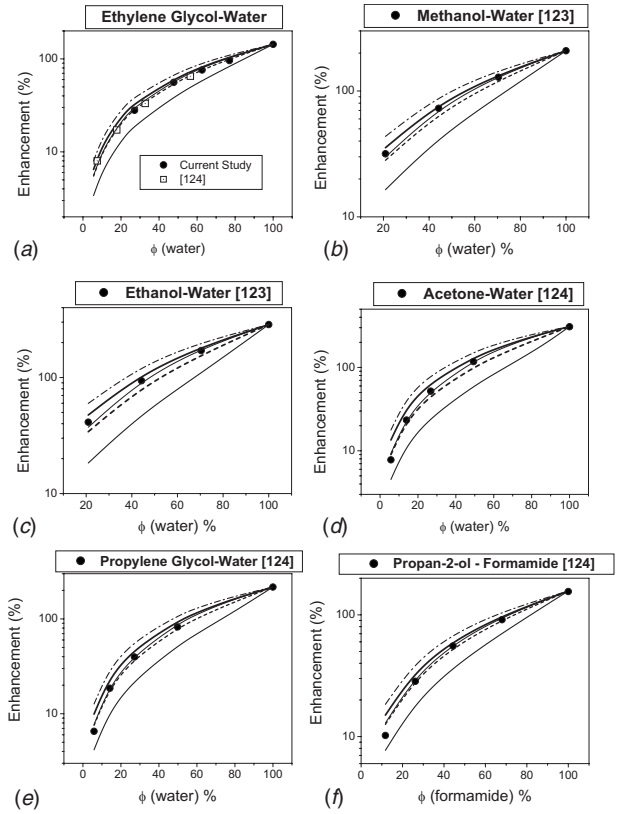

Fig. 7 Classical bounds for thermal conductivity in liquid mixtures. The line and symbol codes are the same as in Fig. 6 with the addition of a thin solid line between the Maxwell bounds, denoting the unbiased or Bruggeman model. Table 2 in the Appendix gives the numerical values used in the calculation of classical bounds. Experimental data are taken from [123], [124], and the current study.

the nanoparticles in the direction of the heat flux. This allows the nanofluid thermal conductivity to increase from the lower Maxwell bound to almost the parallel mode limit. Similar enhancements (of smaller proportions) are also observed for magnetic Fe-water nanofluids [125]. If, however, the magnetic field is applied *perpendicular* to the heat flux, the nanoparticles will stay

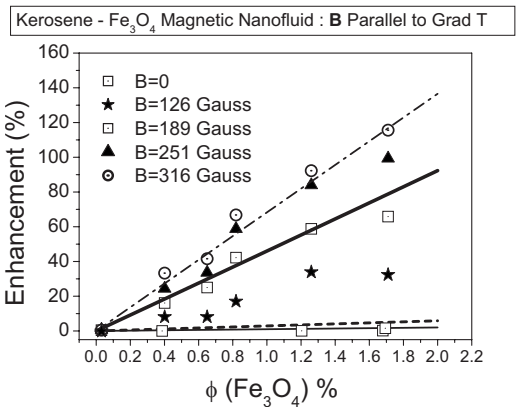

Fig. 8 Thermal conductivity of Kerosene–Fe_3O_4 magnetic nanofluid, as a function of the external magnetic field (B) in the direction of the heat flux (data from Ref. [45]). The configuration of the nanoparticles range from dispersed arrangement (at low B) to the chainlike formation in the direction of the heat flux (at high B). The line and symbol codes are the same as in Fig. 6. The classical bounds are calculated based on the data listed in Table 3 of the Appendix.

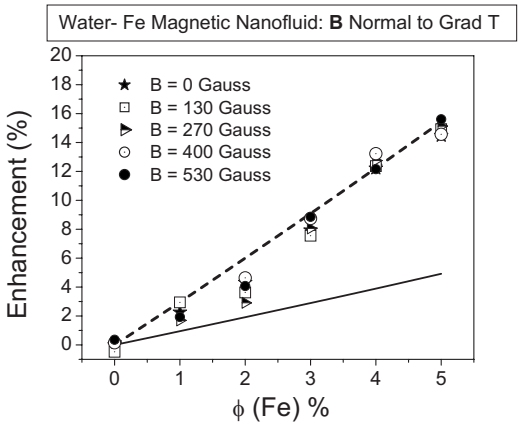

Fig. 9 Thermal conductivity of water–Fe magnetic nanofluid as a function of the external magnetic field (B) perpendicular to the direction of the heat flow (data from Ref. [125]). The nanoparticles are dispersed or form clusters perpendicular to the heat flux. The dashed and solid lines correspond to the lower Maxwell and series bounds, respectively. The classical bounds are calculated based on the data listed in Table 3 of the Appendix.

dispersed or clustered in a direction normal to the heat flux. In this case, the classical theory predicts that the enhancement will be bounded by the series mode limit and the *lower* Maxwell bound. Indeed, the experimental observation of Li et al. [125] conforms to this prediction, as shown in Fig. 9. The experiments performed with magnetic nanofluids (in magnetic fields) provide the most direct and unambiguous evidence for the effect of linear or fractal-like clustering on the nanofluid thermal conductivity.

Next, in Fig. 10, we delineate the classical bounds for a large set of nanofluids including those which have been described as unusual or anomalous. The data sets include oxide nanoparticles with relatively low κ (silica and zirconia), moderate κ (alumina and copper oxide), and high κ (copper, aluminum, and carbon nanotubes). They also include different base media including water (polar), ethylene glycol, and oil, and nanoparticles with a lower thermal conductivity relative to the base media (C-60/70 and MFA in water). Quite remarkably, all the data, except for a few sets, lie between the upper and lower Maxwell bounds, affirming the same mechanism for thermal conduction for nanofluids as that for solid composites and liquid mixtures, namely, through molecular or electronic interactions. By examining the main features of the nanofluid data, we can derive useful insights into the finer details of the conduction mechanism.

The most striking feature is that only a small set of nanofluid data falls significantly below the lower Maxwell bound even at very low volume fractions and with nanoparticle diameters that are in the tens of nanometers. This behavior is very unlike that in solid composites, where at low volume fractions and with nanometer sized filler particles, the effective thermal conductivity drop well below the series conduction bound. When the thermal conductivity of the dispersed media becomes closer to that of the base media, the Maxwell bounds becomes narrower, as can be noted with silica, zirconia, and Fe_3O_4. This also implies that uncertainties in nanoparticle thermal conductivity can cause discernible changes in the Maxwell bounds when $\kappa_p - \kappa_f$ is small. For most nanofluids, however, the difference is large. The lower Maxwell bound represents the maximum thermal conductivity that is possible with well-dispersed nanoparticles, and it can be inferred that the interfacial thermal resistance for most nanofluids is negligible (exceptions are noted, for example, in Ref. [24]). Even if the nanoparticle thermal conductivity is smaller than that of the bulk value (as observed in nanosized thin films [126]), all the experimental data, except for fullerenes (C-60/70) and to some extent,

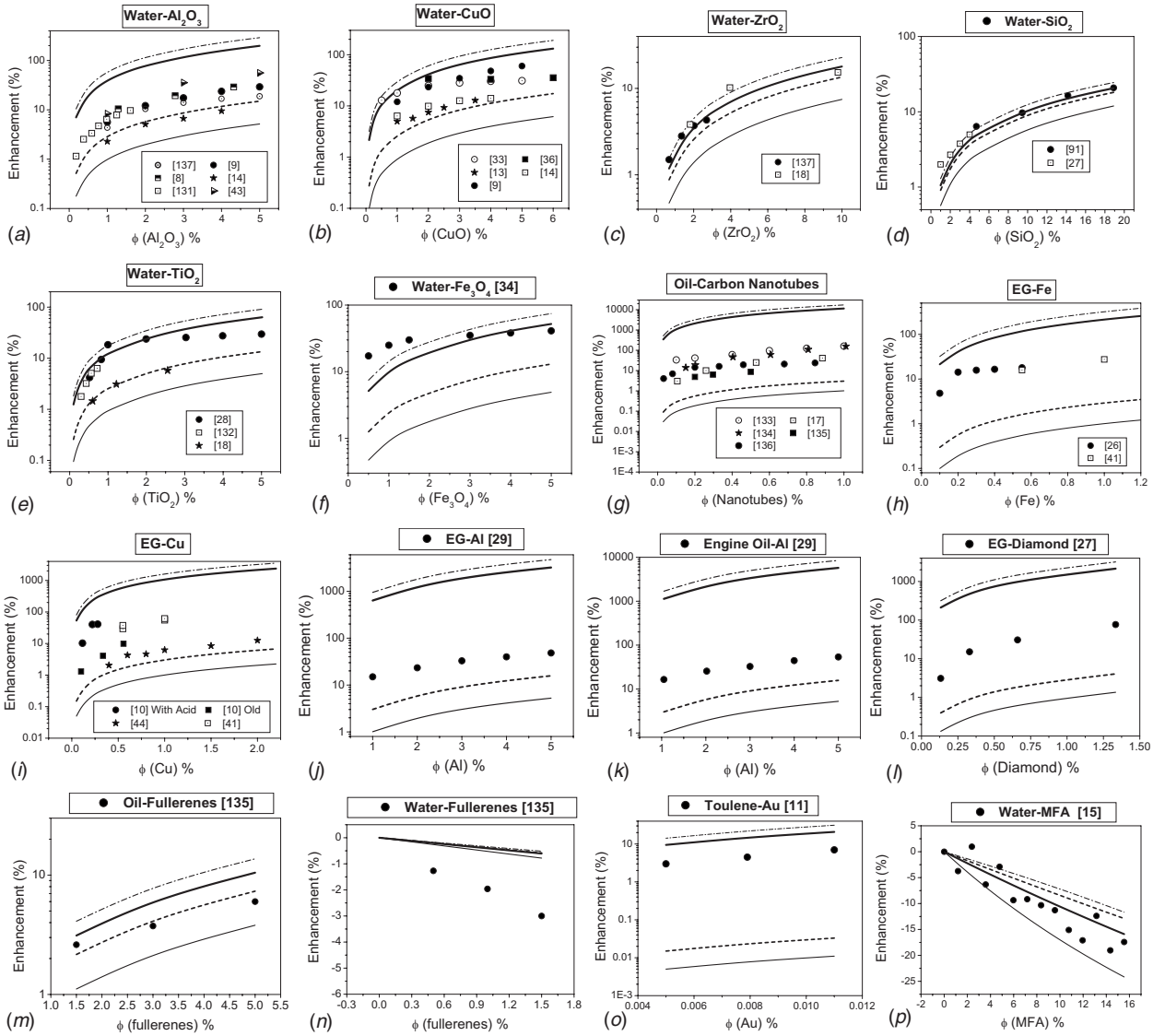

Fig. 10 The classical bounds for thermal conductivity/diffusivity in nanofluids. The line and symbol codes are the same as in Fig. 6. Since thermal conductivities of the dispersed media (nanoparticles) are generally not measured or reported, representative values listed in Table 3 of the Appendix are used to compute for the classical bounds. It is observed that $\kappa_p \gg \kappa_f$ for most nanofluids. The bounds shown are for a given temperature, while the experimental data shown may not correspond to the same temperature. This is largely of no consequence, given the rather small deviation in base fluid thermal conductivity in the range of experimentation. The assessment that most nanofluids respect the classical bounds, therefore, remains unchanged even after factoring in different experimental temperatures, and uncertainties in the experimental methods [46] and thermal conductivities. Experimental data are taken from [8–11], [13–15], [17], [18], [26–29], [33], [34], [36], [41], [43], [44], [91], and [131–137].

MFA, remain bounded by the lower Maxwell bound with $R_b=0$.

The occurrence of an interfacial thermal (Kapitza) resistance at a liquid-solid interface has been experimentally evaluated by Ge et al. [127], who observed a bounding R_b of 0.67×10^{-8} $\mathrm{Km^2W^{-1}}$ and 2×10^{-8} $\mathrm{Km^2W^{-1}}$ for hydrophilic and hydrophobic interfaces, respectively. With nanofluids with carbon nanotubes, a large variation in R_b, ranging from a low 0.24×10^{-8} $\mathrm{Km^2W^{-1}}$ [128] to a high 8.3×10^{-8} $\mathrm{Km^2W^{-1}}$ [129,130] is also reported. The high values are comparable to those in a solid matrix, such as in diamond-silicon composite with a R_b of 27×10^{-8} $\mathrm{Km^2W^{-1}}$ [126]. The large span in the R_b data for carbon nanotube suspensions, and the near zero R_b for most other nanofluids indicate the role of solid-fluid interactions on the interfacial thermal resistance. Theoretical studies show that R_b attains relatively large values only when the liquid does not wet the solid surface. In our context, complete wetting may be a reasonable assumption for dispersions of hydrophylic colloids such as Ludox, and possibly for charged MFA colloids, where particle solvation is ensured by electrostatic forces. We also point out that terms such as "hydrophobic" and "hydrophilic" are rather subtle, and the macroscopic concepts such as the contact angle may be a bit misleading. The rate of energy transfer would be indeed weaker if the liquid does not wet the solid, since in this case the liquid density in the interfacial layer would be depleted. Yet, from a microscopic point of view, what one may need to consider is the free energy of insertion of the particle in the fluid. For a stable, nonaggregating colloidal dispersion, the latter is certainly negative (meaning, the particles are well-solvated). This means that even particles made of a hydrophobic material such as MFA can behave as hydrophilic. The reason for this apparent paradox is related to the presence of the charged double-layer, which leads to the formation of a solvation layer made of hydrated counterions, hindering solvent

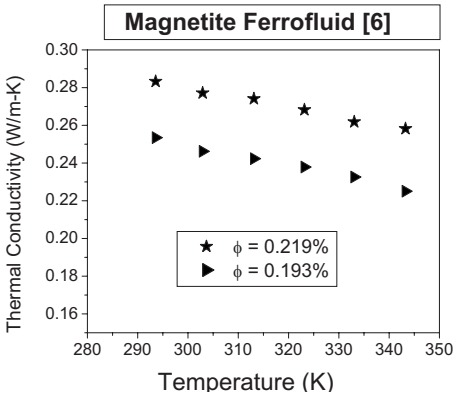

Fig. 11 Temperature dependence of magnetite nanofluid thermal conductivity [6]. While no strong correlation is generally observed to the thermal motion of the nanoparticles, there appears to be a dependence on the thermal conductivity variation of the base fluid. The base fluid (transformer oil) thermal conductivity decreases slightly with temperature for the range of temperatures shown [6].

depletion in the interfacial layer. This is partially evident by the very different behavior for fullerenes (C-60/70) suspensions in surfactant-stabilized water, and oil without the use of a surfactant. While for fullerenes in water, a small, but identifiable reduction in thermal conductivity below the Maxwell prediction is recorded, possibly due to the interactions of surfactant molecules with surrounding liquid, fullerenes in oil is consistent with Maxwell prediction with $R_b=0$.

Several of the reported anomalous characteristics such as the lack of correlation to particle thermal conductivity and size effects can be resolved by weighing in the ability of nanoparticles into forming linear chainlike aggregates. Not all aggregates are equally efficient in increasing the thermal conductivity as experiments show that the larger clusters without the linear chain-forming configurations lead to a limiting behavior in the enhancement [52]. The temperature dependence is also not as striking as it was earlier believed with the recent experiments [137,138] showing a similar variation for both nanofluids and the base fluid. This implies that the mechanism for the increase in the thermal conductivity of water (for example, the temperature dependent slow modes [139]) is responsible for the thermal conductivity increase in the colloidal state as well. Conversely, it is reasonable to expect a *decrease* in the nanofluid thermal conductivity for a base fluid that has a negative change in thermal conductivity with increasing temperature. Early experiments on ferrofluids [6], indeed, have demonstrated this behavior, as shown in Fig. 11.

5 Concluding Remarks

The classical Maxwell theory has two limiting bounds that correspond to two geometrical nanoparticle configurations in the colloidal state. For the first bound, nanoparticles form the dispersed phase and the fluid medium acts as the continuous phase, while for the second the roles are reversed with the nanoparticles and the fluid medium constituting the continuous and dispersed phases, respectively. For the latter, the nanoparticles *must* form linear or fractal configurations, which separate the large regions of fluid pockets.

By analyzing a large body of data including those from our own experiments, we show that almost all the reported thermal conductivity data are enveloped by the upper and lower Maxwell bounds. For a homogeneous nanofluid system, these bounds set the limits for thermal conductivity enhancements. The thermal conductivity for the upper bound is maximally biased toward the thermal conductivity of the nanoparticles and *vice versa* for the lower bound. Experimental data on nanofluids, solid composites, and liquid mixtures indicate that the upper and lower Maxwell bounds are universally respected by most binary composites, regardless of the physical state and the thermal conductivity of the phases. The striking similarity of the nanofluid data to those of solid composites and liquid mixtures strongly indicate that the mechanism of nanofluid thermal conductivity is classical in nature, namely, through molecular and electronic interactions.

The earlier reports of anomalously high thermal conductivity can be traced back to an exclusive comparison of the test data to models, which are applicable only to well-dispersed nanoparticles. Once this constraint is relaxed, and a linear chain or fractal configuration is allowed for the nanoparticles, the classical models can predict a thermal conductivity range that easily accommodates almost all the experimental data. A key difference between the thermal conduction behavior in nanofluids and solid composites appears to be the interfacial thermal resistance. A large body of nanofluid experimental data suggests that the interfacial thermal resistance is negligible for most nanofluids.

On the basis of the experimental evidences provided in this paper, the key to having an enhanced thermal conductivity lies on the aggregation state and connectivity of the nanoparticles With the current experimental techniques such as neutron scattering, it is possible to characterize the aggregation state in the colloidal state. Once these geometrical details are available, a more precise comparison can be made between several samples (of the same constituents), which show appreciable differences in the thermal conductivity. While the science of making well-dispersed colloids has reached a fair amount of maturity, the techniques for developing targeted nanoparticle configurations are still in an evolving phase. It is expected that future studies can systematically address the configurational constraints necessary for enhanced thermal transport in nanofluids.

Acknowledgment

J.E. wishes to thank John Philip, Jacopo Buongiorno, Wesley Williams, Pawel Keblinski, and Ravi Prasher for their insightful discussions on nanofluids.

Appendix

Tables 1–3 show the thermal conductivity data for solid composites, liquid mixtures and nanofluids.

Table 1 Thermal conductivity data for solid composites

Material	κ (W/m -K)	Reference
Aluminum	237	[117]
Alumina	33.095	[120]
Graphite	209.2	[120]
Cupric oxide	9.21	[116]
Copper	384	[56,118]
Aluminum nitride	200	[140]
Diamond (polycrystal)	600	[55]
Zn	116	[56]
Polypropylene	0.239	[117]
Polyethylene	0.505/0.291	[56,120]
Epoxy	0.221	[116]
Polyamide	0.32	[118]
Polyvinylidene fluoride	0.12	[119]
Zinc sulphide	17.4	[55]

Table 2 Thermal conductivity data for liquid mixtures

Material	κ (W/m -K)	Reference
Water	0.61	25°C, [141]
Ethanol	0.161	32.6°C, [123]
Acetone	0.154	40°C, [124]
Methanol	0.198	28.1°C, [123]
Propylene glycol	0.199	40°C, [124]
Ethylene glycol	0.252	40°C, [124]
Propan-2-ol	0.137	40°C, [124]
Formamide	0.352	40°C, [124]

Table 3 Thermal conductivity data for nanofluids

Material	κ (W/m -K)	Reference
Water	0.61	25°C, [141]
Ethylene glycol (EG)	0.26	25°C, Measured value [142]
Oil	0.11–0.15	Representative range [133–135]
Al_2O_3	35	Representative value, [120,143]
CuO	20	Representative value, [144]
ZrO_2	2	Representative value, [145]
TiO_2	11.7	Representative value, [145]
SiO_2	1.4	Representative value, [91,135]
Fe_3O_4	9.7	[146,147]
Au	317	[143]
Ag	429	[143]
Al	237	[143]
Fe	80.2	[143]
Carbon nanotubes (CNT)	2000	Representative value, [134]
Diamond	600	Polycrystalline, [55]
Fullerenes (C_{60})	0.4	[148]
MFA	0.2	[91]

References

[1] Weitz, D. A., Huang, J. S., Lin, M. Y., and Sung, J., 1984, "Dynamics of Diffusion-Limited Kinetic Aggregation," Phys. Rev. Lett., **53**, pp. 1657–1660.

[2] Weitz, D. A., Huang, J. S., Lin, M. Y., and Sung, J., 1985, "Limits of the Fractal Dimension for Irreversible Kinetic Aggregation of Gold Colloids," Phys. Rev. Lett., **54**, pp. 1416–1419.

[3] Weitz, D. A., and Oliveria, M., 1984, "Fractal Structures Formed by Kinetic Aggregation of Aqueous Gold Colloids," Phys. Rev. Lett., **52**, pp. 1433–1436.

[4] Meakin, P., 1992, "Aggregation Kinetics," Phys. Scr., **46**, pp. 295–331.

[5] Fertman, V. E., 1987, "Thermal and Physical Properties of Magnetic Fluids," J. Eng. Phys. Thermophys., **53**, pp. 1097–1105.

[6] Fertman, V. E., Golovicher, L. E., and Matusevich, N. P., 1987, "Thermal Conductivity of Magnetite Magnetic Fluids," J. Magn. Magn. Mater., **65**, pp. 211–214.

[7] Popplewell, J., Al-Qenaie, A., Charles, S. W., Moskowitz, R., and Raj, K., 1982, "Thermal Conductivity Measurements on Ferrofluids," Colloid Polym. Sci., **260**, pp. 333–338.

[8] Masuda, H., Ebata, A., Teramae, K., and Hishinuma, N., 1993, "Alteration of Thermal Conductivity and Viscosity of Liquid by Dispersing Ultra-Fine Particles (Dispersion of γ-Al_2O_3, SiO_2, and TiO_2 Ultra-Fine Particles)," Netsu Bussei, **7**, pp. 227–233.

[9] Eastman, J. A., Choi, S. U. S., Li, S., Thompson, L. J., and Lee, S., 1997, "Enhanced Thermal Conductivity Through the Development of Nanofluids," Mater. Res. Soc. Symp. Proc., **457**, pp. 3–11.

[10] Eastman, J. A., Choi, S. U. S., Li, S., Yu, W., and Thompson, L. J., 2001, "Anomalously Increased Effective Thermal Conductivities of Ethylene Glycol-Based Nanofluids Containing Copper Nanoparticles," Appl. Phys. Lett., **78**, pp. 718–720.

[11] Patel, H. E., Das, S. K., Sundararajan, T., Nair, A. S., George, B., and Pradeep, T., 2003, "Thermal Conductivities of Naked and Monolayer Protected Metal Nanoparticle Based Nanofluids: Manifestation of Anomalous Enhancement and Chemical Effects," Appl. Phys. Lett., **83**, pp. 2931–2933.

[12] Wang, X., Xu, X., and Choi, S. U. S., 1999, "Thermal Conductivity of Nanoparticle-Fluid Mixture," J. Thermophys. Heat Transfer, **13**, pp. 474–480.

[13] Lee, S., Choi, S. U. S., Li, S., and Eastman, J. A., 1999, "Measuring Thermal Conductivity of Fluids Containing Oxide Nanoparticles," ASME J. Heat Transfer, **121**, pp. 280–289.

[14] Das, S. K., Putra, N., Thiesen, P., and Roetzel, W., 2003, "Temperature Dependence of Thermal Conductivity Enhancement for Nanofluids," ASME J. Heat Transfer, **125**, pp. 567–574.

[15] Rusconi, R., Rodari, E., and Piazza, R., 2006, "Optical Measurements of the Thermal Properties of Nanofluids," Appl. Phys. Lett., **89**, p. 261916.

[16] Venerus, D. C., Kabadi, M. S., Lee, S., and Perez-Luna, V., 2006, "Study of Thermal Transport in Nanoparticle Suspensions Using Forced Rayleigh Scattering," J. Appl. Phys., **100**, p. 094310.

[17] Zhang, X., Gu, H., and Fujii, M., 2006, "Effective Thermal Conductivity and Thermal Diffusivity of Nanofluids Containing Spherical and Cylindrical Nanoparticles," J. Appl. Phys., **100**, p. 044325.

[18] Zhang, X., Gu, H., and Fujii, M., 2006, "Experimental Study on the Effective Thermal Conductivity and Thermal Diffusivity of Nanofluids," Int. J. Thermophys., **27**, pp. 569–580.

[19] Xie, H., Wang, J., Xi, T., and Liu, Y., 2002, "Thermal Conductivity of Suspensions Containing Nanosized SiC Particles," Int. J. Thermophys., **23**, pp. 571–580.

[20] Putnam, S. A., Cahill, D. G., Braun, P. V., Ge, Z., and Shimmin, R. G., 2006, "Thermal Conductivity of Nanoparticle Suspensions," J. Appl. Phys., **99**, p. 084308.

[21] Keblinski, P., Eastman, J. A., and Cahill, D. G., 2005, "Nanofluids for Thermal Transport," Mater. Today, **8**, pp. 36–44.

[22] Singh, D., Timofeeva, E., Yu, W., Routbort, J., France, D., Smith, D., and Lopez-Cepero, J. M., 2009, "An Investigation of Silicon Carbide-Water Nanofluid for Heat Transfer Applications," J. Appl. Phys., **105**, p. 064306.

[23] Ju, Y. S., Kim, J., and Hung, M.-T., 2008, "Experimental Study of Heat Conduction in Aqueous Suspensions of Aluminum Oxide Nanoparticles," ASME J. Heat Transfer, **130**, p. 092403.

[24] Timofeeva, E. V., Gavrilov, A. N., McCloskey, J. M., Tolmachev, Y. V., Sprunt, S., Lopatina, L. M., and Selinger, J. V., 2007, "Thermal Conductivity and Particle Agglomeration in Alumina Nanofluids: Experiment and Theory," Phys. Rev. E, **76**, p. 061203.

[25] Chon, C. H., Kihm, K. D., Lee, S. P., and Choi, S. U. S., 2005, "Empirical Correlation Finding the Role of Temperature and Particle Size for Nanofluid (Al_2O_3) Thermal Conductivity Enhancement," Appl. Phys. Lett., **87**, p. 153107.

[26] Hong, T. K., Yang, H. S., and Choi, C. J., 2005, "Study of the Enhanced Thermal Conductivity of Fe Nanofluids," J. Appl. Phys., **97**, p. 064311.

[27] Kang, H. U., Kim, S. H., and Oh, J. M., 2006, "Estimation of Thermal Conductivity of Nanofluid Using Experimental Effective Particle Volume," Exp. Heat Transfer, **19**, pp. 181–191.

[28] Murshed, S. M. S., Leong, K. C., and Yang, C., 2005, "Enhanced Thermal Conductivity of TiO_2-Water Based Nanofluids," Int. J. Therm. Sci., **44**, pp. 367–373.

[29] Murshed, S. M. S., Leong, K. C., and Yang, C., 2006, "Determination of the Effective Thermal Diffusivity of Nanofluids by the Double Hot-Wire Technique," J. Phys. D, **39**, pp. 5316–5322.

[30] Chopkar, M., Das, P. K., and Manna, I., 2006, "Synthesis and Characterization of Nanofluid for Advanced Heat Transfer Applications," Scr. Mater., **55**, pp. 549–552.

[31] Chopkar, M., Kumar, S., Bhandari, D. R., Das, P. K., and Manna, I., 2007, "Development and Characterization of Al_2Cu and Ag_2Al Nanoparticle Dispersed Water and Ethylene Glycol Based Nanofluid," Mater. Sci. Eng., B, **139**, pp. 141–148.

[32] Li, C. H., and Peterson, G. P., 2007, "The Effect of Particle Size on the Effective Thermal Conductivity of Al_2O_3-Water Nanofluids," J. Appl. Phys., **101**, p. 044312.

[33] Zhu, H. T., Zhang, C. Y., Tang, Y. M., and Wang, J. X., 2007, "Novel Synthesis and Thermal Conductivity of CuO Nanofluid," J. Phys. Chem. C, **111**, pp. 1646–1650.

[34] Zhu, H., Zhang, C., Liu, S., Tang, Y., and Yin, Y., 2006, "Effects of Nanoparticle Clustering and Alignment on Thermal Conductivities of Fe_3O_4 Aqueous Nanofluids," Appl. Phys. Lett., **89**, pp. 023123.

[35] Li, Q., and Xuan, Y., 2006, "Enhanced Heat Transfer Behaviors of New Heat Carrier for Spacecraft Thermal Management," J. Spacecr. Rockets, **43**, pp. 687–689.

[36] Li, C. H., and Peterson, G. P., 2006, "Experimental Investigation of Temperature and Volume Fraction Variations on the Effective Thermal Conductivity of Nanoparticle Suspensions (Nanofluids)," J. Appl. Phys., **99**, p. 084314.

[37] Yoo, D.-H., Hong, K. S., and Yang, H.-S., 2007,"Study of Thermal Conductivity of Nanofluids for the Application of Heat Transfer Fluids," Thermochim. Acta, **455**, pp. 66–69.

[38] Vázquez Peñas, J. R., Ortiz de Zárate, J. M., and Khayet, M., 2008, "Measurement of the Thermal Conductivity of Nanofluids by the Multicurrent Hot-Wire Method," J. Appl. Phys., **104**, p. 044314.

[39] Philip, J., Shima, P. D., and Raj, B., 2008, "Nanofluid With Tunable Thermal Properties," Appl. Phys. Lett., **92**, p. 043108.

[40] Schmidt, A. J., Chiesa, M., Torchinsky, D. H., Johnson, J. A., Nelson, K. A., and Chen, G., 2008, "Thermal Conductivity of Nanoparticle Suspensions in Insulating Media Measured With a Transient Optical Grating and a Hotwire," J. Appl. Phys., **103**, p. 083529.

[41] Sinha, K., Kavlicoglu, B., Liu, Y., Gordaninejad, F., and Graeve, O. A., 2009, "A Comparative Study of Thermal Behavior of Iron and Copper Nanofluids," J. Appl. Phys., **106**, p. 064307.

[42] Shima, P. D., Philip, J., and Raj, B., 2009, "Role of Microconvection Induced by Brownian Motion of Nanoparticles in the Enhanced Thermal Conductivity of Stable Nanofluids," Appl. Phys. Lett., **94**, p. 223101.

[43] Gharagozloo, P. E., Eaton, J. K., and Goodson, K. E., 2008, "Diffusion, Aggregation, and the Thermal Conductivity of Nanofluids," Appl. Phys. Lett., **93**, p. 103110.

[44] Garg, J., Poudel, B., Chiesa, M., Gordon, J. B., Ma, J. J., Wang, J. B., Ren, Z. F., Kang, Y. T., Ohtani, H., Nanda, J., McKinley, G. H., and Chen, G., 2008, "Enhanced Thermal Conductivity and Viscosity of Copper Nanoparticles in Ethylene Glycol Nanofluid," J. Appl. Phys., **103**, p. 074301.
[45] Philip, J., Shima, P. D., and Raj, B., 2007, "Enhancement of Thermal Conductivity in Magnetite Based Nanofluid due to Chainlike Structures," Appl. Phys. Lett., **91**, p. 203108.
[46] Buongiorno, J., Venerus, D. C., Prabhat, N., McKrell, T., Townsend, J., Christianson, R., Tolmachev, Y. V., Keblinski, P., Hu, L.-W., Alvarado, J. L., Bang, I. C., Bishnoi, S. W., Bonetti, M., Botz, F., Cecere, A., Chang, Y., Chen, G., Chung, S. J., Chyu, M. K., Das, S. K., Di Paola, R., Ding, Y., Dubois, F., Dzido, G., Eapen, J., Escher, W., Funfschilling, D., Galand, Q., Gao, J., Gharagozloo, P. E., Goodson, K. E., Gutierrez, J. G., Hong, H., Horton, M., Hwang, K. S., Iorio, C. S., Jang, S. P., Jarzebski, A. B., Jiang, Y., Jin, L., Kabelac, S., Kamath, A., Kedzierski, M. A., Kieng, L. G., Kim, C., Kim, J.-H., Kim, S., Lee, S. H., Leong, K. C., Manna, I., Michel, B., Ni, R., Patel, H. E., Philip, J., Poulikakos, D., Reynaud, C., Savino, R., Savino, R., Singh, P. K., Song, P., Sundararajan, T., Timofeeva, E., Tritcak, T., Turanov, A. N., Van Vaerenbergh, S., Wen, D., Witharana, S., Yang, C., Yeh, W.-H., Zhao, X.-Z., and Zhou, S.-Q., 2009, "A Benchmark Study on the Thermal Conductivity of Nanofluids," J. Appl. Phys., **106**, p. 094312.
[47] Maxwell, J. C., 1881, *A Treatise on Electricity and Magnetism*, Vol. 1, 2nd ed., Claredon, Oxford.
[48] Hashin, Z., and Shtrikman, S., 1962, "A Variational Approach to the Theory of the Effective Magnetic Permeability of Multiphase Materials," J. Appl. Phys., **33**, pp. 3125–3131.
[49] Nan, C.-W., Birringer, R., Clarke, D. R., and Gleiter, H., 1997, "Effective Thermal Conductivity of Particulate Composites With Interfacial Thermal Resistance," J. Appl. Phys., **81**, pp. 6692–6699.
[50] Benveniste, Y., 1987, "Effective Thermal Conductivity of Composites With a Thermal Contact Resistance Between the Constituents: Nondilute Case," J. Appl. Phys., **61**, pp. 2840.
[51] Kim, S. H., Choi, S. R., and Kim, D., 2007, "Thermal Conductivity of Metal-Oxide Nanofluids: Particle Size Dependence and Effect of Laser Irradiation," ASME J. Heat Transfer, **129**, pp. 298–307.
[52] Hong, K. S., Hong, T.-K., and Yang, H.-S., 2006, "Thermal Conductivity of Fe Nanofluids Depending on the Cluster Size of Nanoparticles," Appl. Phys. Lett., **88**, p. 031901.
[53] Li, C. H., Williams, W., Buongiorno, J., Hu, L.-W., and Peterson, G. P., 2008, "Transient and Steady-State Experimental Comparison Study of Effective Thermal Conductivity of Al_2O_3/Water Nanofluids," ASME J. Heat Transfer, **130**, p. 042407.
[54] Jha, N., and Ramaprabhu, S., 2009, "Thermal Conductivity Studies of Metal Dispersed Multiwalled Carbon Nanotubes in Water and Ethylene Glycol Based Nanofluids," J. Appl. Phys., **106**, p. 084317.
[55] Every, A. G., Tzou, Y., Hasselman, D. P. H., and Raj, R., 1992, "The Effect of Particle Size on the Thermal Conductivity of ZnS/Diamond Composites," Acta Metall. Mater., **40**, pp. 123–129.
[56] Sofian, N. M., Rusu, M., Neagu, R., and Neagu, E., 2001, "Metal Powder-Filled Polyethylene Composites. V. Thermal Properties," J. Thermoplastic Composite Materials, **14**, pp. 20–33.
[57] Hasselman, D. P. H., and Donaldson, K. Y., 2000, "Role of Size in the Effective Thermal Conductivity of Composites With an Interfacial Thermal Barrier," J. Wide Bandgap Mater., **7**, pp. 306–318.
[58] Geiger, A. L., Hasselman, D. P. H., and Donaldson, K. Y., 1993, "Effect of Reinforcement Particle Size on the Thermal Conductivity of a Particulate Silicon-Carbide Reinforced Aluminum-Matrix Composite," J. Mater. Sci. Lett., **12**, pp. 420–423.
[59] Pal, R., 2007, "New Models for Thermal Conductivity of Particulate Composites," J. Reinf. Plast. Compos., **26**, pp. 643–651.
[60] Zhang, H., Ge, X., and Ye, H., 2005, "Effectiveness of the Heat Conduction Reinforcement of Particle Filled Composites," Modell. Simul. Mater. Sci. Eng., **13**, pp. 401–412.
[61] Kumar, D. H., Patel, H. E., Kumar, V. R. R., Sundararajan, T., Pradeep, T., and Das, S. K., 2004, "Model for Heat Conduction in Nanofluids," Phys. Rev. Lett., **93**, p. 144301.
[62] Bhattacharya, P., Saha, S. K., Yadav, A., Phelan, P. E., and Prasher, R. S., 2004, "Brownian Dynamics Simulation to Determine the Effective Thermal Conductivity of Nanofluids," J. Appl. Phys., **95**, pp. 6492–6494.
[63] Koo, J., and Kleinstreuer, C., 2004, "A New Thermal Conductivity Model for Nanofluids," J. Nanopart. Res., **6**, pp. 577–588.
[64] Jang, S. P., and Choi, S. U. S., 2004, "Role of Brownian Motion in the Enhanced Thermal Conductivity of Nanofluids," Appl. Phys. Lett., **84**, pp. 4316–4318.
[65] Jang, S. P., and Choi, S. U. S., 2007, "Effects of Various Parameters on Nanofluid Thermal Conductivity," ASME J. Heat Transfer, **129**, pp. 617–623.
[66] Prasher, R., Bhattacharya, P., and Phelan, P. E., 2005, "Thermal Conductivity of Nanoscale Colloidal Solutions (Nanofluids)," Phys. Rev. Lett., **94**, p. 025901.
[67] Prasher, R., Bhattacharya, P., and Phelan, P. E., 2006, "Brownian-Motion-Based Convective-Conductive Model for the Effective Thermal Conductivity of Nanofluids," ASME J. Heat Transfer, **128**, pp. 588–595.
[68] Li, C. H., and Peterson, G. P., 2007, "Mixing Effect on the Enhancement of the Effective Thermal Conductivity of Nanoparticle Suspensions (Nanofluids)," Int. J. Heat Mass Transfer, **50**, pp. 4668–4677.
[69] Patel, H. E., Sundararajan, T., Pradeep, T., Dasgupta, A., Dasgupta, N., and Das, S. K., 2005, "A Micro-Convection Model for Thermal Conductivity of Nanofluids," Pramana, J. Phys., **65**, pp. 863–869.
[70] Yu, W., and Choi, S. U. S., 2003, "The Role of Interfacial Layers in the Enhanced Thermal Conductivity of Nanofluids: A Renovated Maxwell Model," J. Nanopart. Res., **5**, pp. 167–171.
[71] Xue, Q.-Z., 2003, "Model for Effective Thermal Conductivity of Nanofluids," Phys. Lett. A, **307**, pp. 313–317.
[72] Xie, H., Fujii, M., and Zhang, X., 2005, "Effect of Interfacial Nanolayer on the Effective Thermal Conductivity of Nanoparticle-Fluid Mixture," Int. J. Heat Mass Transfer, **48**, pp. 2926–2932.
[73] Xue, Q., and Xu, W.-M., 2005, "A Model of Thermal Conductivity of Nanofluids With Interfacial Shells," Mater. Chem. Phys., **90**, pp. 298–301.
[74] Tillman, P., and Hill, J. M., 2007, "Determination of Nanolayer Thickness for a Nanofluid," Int. Commun. Heat Mass Transfer, **34**, pp. 399–407.
[75] Avsec, J., and Oblak, M., 2007, "The Calculation of Thermal Conductivity, Viscosity and Thermodynamic Properties for Nanofluids on the Basis of Statistical Nanomechanics," Int. J. Heat Mass Transfer, **50**, pp. 4331–4341.
[76] Gao, L., and Zhou, X. F., 2006, "Differential Effective Medium Theory for Thermal Conductivity in Nanofluids," Phys. Lett. A, **348**, pp. 355–360.
[77] Zhou, X. F., and Gao, L., 2006, "Effective Thermal Conductivity in Nanofluids of Nonspherical Particles With Interfacial Thermal Resistance: Differential Effective Medium Theory," J. Appl. Phys., **100**, p. 024913.
[78] Prasher, R., Evans, W., Meakin, P., Fish, J., Phelan, P., and Keblinski, P., 2006, "Effect of Aggregation on Thermal Conduction in Colloidal Nanofluids," Appl. Phys. Lett., **89**, p. 143119.
[79] Jie, X., Yu, B.-M., and Yun, M.-J., 2006, "Effect of Clusters on Thermal Conductivity in Nanofluids," Chin. Phys. Lett., **23**, pp. 2819–2822.
[80] Feng, Y., Yu, B., Xu, P., and Zou, M., 2007, "The Effective Thermal Conductivity of Nanofluids Based on the Nanolayer and the Aggregation of Nanopartciles," J. Phys. D: Appl. Phys., **40**, pp. 3164–3171.
[81] Xu, J., Yu, B., Zou, M., and Xu, P., 2006, "A New Model for Heat Conduction of Nanofluids Based on Fractal Distributions of Nanoparticles," J. Phys. D, **39**, pp. 4486–4490.
[82] Ren, Y., Xie, H., and Cai, A., 2005, "Effective Thermal Conductivity of Nanofluids Containing Spherical Nanoparticles," J. Phys. D, **38**, pp. 3958–3961.
[83] Wang, B.-X., Zhou, L.-P., and Peng, Z.-F., 2003, "A Fractal Model for Predicting the Effective Thermal Conductivity of Liquid With Suspension of Nanoparticles," Int. J. Heat Mass Transfer, **46**, pp. 2665–2672.
[84] Xuan, Y., Li, Q., and Hu, W., 2004, "Aggregation Structure and Thermal Conductivity of Nanofluids," AIChE J., **49**, pp. 1038–1043.
[85] Prasher, R., Phelan, P. E., and Bhattacharya, P., 2006, "Effect of Aggregation Kinetics on the Thermal Conductivity of Nanoscale Colloidal Solutions (Nanofluid)," Nano Lett., **6**, pp. 1529–1534.
[86] Keblinski, P., Prasher, R., and Eapen, J., 2008, "Thermal Conductance of Nanofluids: Is the Controversy Over?," J. Nanopart. Res., **10**, pp. 1089–1097.
[87] deGroot, S. R., and Mazur, P., 1984, *Nonequilibrium Thermodynamics*, Dover, New York.
[88] DeVera, A. L., and Strieder, W., 1977, "Upper and Lower Bounds on the Thermal Conductivity of a Random, Two-Phase Material," J. Phys. Chem., **81**, pp. 1783.
[89] Carson, J. K., Lovatt, S. J., Tanner, D. J., and Cleland, A. C., 2005, "Thermal Conductivity Bounds for Isotropic Porous Materials," Int. J. Heat Mass Transfer, **48**, pp. 2150–2158.
[90] Griesinger, A., Hurler, W., and Pietralla, M., 1997, "A Photothermal Method With Step Heating for Measuring the Thermal Diffusivity of Anisotropic Solids," Int. J. Heat Mass Transfer, **40**, pp. 3049–3058.
[91] Eapen, J., Williams, W. C., Buongiorno, J., Hu, L.-W., Yip, S., Rusconi, R., and Piazza, R., 2007, "Mean-Field Versus Microconvection Effects in Nanofluid Thermal Conduction," Phys. Rev. Lett., **99**, p. 095901.
[92] Torquato, S., and Rintoul, M. D., 1995, "Effect of Interface on the Properties of Composite Media," Phys. Rev. Lett., **75**, pp. 4067–4070.
[93] Raghavan, K., Foster, K., Motakabbir, K., and Berkowitz, M., 1991, "Structure and Dynamics of Water at the Pt(111) Interface: Molecular Dynamics Study," J. Chem. Phys., **94**, pp. 2110–2117.
[94] Reedijk, M. F., Arsic, J., Hollander, F. F. A., de Vries, S. A., and Vlieg, E., 2003, "Liquid Order at the Interface of KDP Crystals With Water: Evidence for Icelike Layers," Phys. Rev. Lett., **90**, p. 066103.
[95] Mo, H., Evmenenko, G., and Dutta, P., 2005, "Ordering of Liquid Squalane Near a Solid Surface," Chem. Phys. Lett., **415**, pp. 106–109.
[96] Yu, C.-J., Richter, A. G., Kmetko, J., Dugan, S. W., Datta, A., and Dutta, P., 2001, "Structure of Interfacial Liquids: X-Ray Scattering Studies," Phys. Rev. E, **63**, p. 021205.
[97] Eapen, J., Li, J., and Yip, S., 2007, "Beyond the Maxwell Limit: Thermal Conduction in Nanofluids With Percolating Fluid Structures," Phys. Rev. E, **76**, p. 062501.
[98] Xue, L., Keblinski, P., Phillpot, S. R., Choi, S. U. S., and Eastman, J. A., 2004, "Effect of Liquid Layering at the Liquid-Solid Interface on Thermal Transport," Int. J. Heat Mass Transfer, **47**, pp. 4277–4284.
[99] Evans, W., Fish, J., and Keblinski, P., 2007, "Thermal Conductivity of Ordered Molecular Water," J. Chem. Phys., **126**, p. 154504.
[100] Mo, H., Evmenenko, G., Kewalramani, S., Kim, K., Ehrlich, S. N., and Dutta, P., 2006, "Observation of Surface Layering in a Nonmetallic Liquid," Phys. Rev. Lett., **96**, p. 096107.
[101] Wang, X.-Q., and Mujumdar, A. S., 2007, "Heat Transfer Characteristics of Nanofluids: A Review," Int. J. Therm. Sci., **46**, pp. 1–19.
[102] Keblinski, P., and Cahill, D. G., 2005, "Comment on "Model for Heat Conduction in Nanofluids"," Phys. Rev. Lett., **95**, p. 209401.
[103] Bastea, S., 2005, "Comment on "Model for Heat Conduction in Nano-

fluids",," Phys. Rev. Lett., **95**, p. 019401.
[104] He, P., and Qiao, R., 2008, "Self-Consistent Fluctuating Hydrodynamics Simulations of Thermal Transport in Nanoparticle Suspensions," J. Appl. Phys., **103**, p. 094305.
[105] Morozov, K. I., 2002, *On the Theory of the Soret Effect in Colloids*, W. Köhler and S. Wiegand, eds., Springer-Verlag, Berlin.
[106] Piazza, R., 2004, "'Thermal Forces': Colloids in Temperature Gradients," J. Phys.: Condens. Matter, **16**, pp. S4195–S4211.
[107] Keblinski, P., Phillpot, S. R., Choi, S. U. S., and Eastman, J. A., 2002, "Mechanisms of Heat Flow in Suspensions of Nano-Sized Particles (Nanofluids)," Int. J. Heat Mass Transfer, **45**, pp. 855–863.
[108] Nie, C., Marlow, W. H., and Hassan, Y. A., 2008, "Discussion of Proposed Mechanisms of Thermal Conductivity Enhancement in Nanofluids," Int. J. Heat Mass Transfer, **51**, pp. 1342–1348.
[109] Hass, K. C., Schneider, W. F., Curioni, A., and Andreoni, W., 1998, "The Chemistry of Water on Alumina Surfaces: Reaction Dynamics From First Principles,"," Science, **282**, pp. 265–268.
[110] Gmachowski, L., 2002, "Aggregate Restructuring and Its Effect on the Aggregate Size Distribution," Colloids Surf., A, **207**, pp. 271–277.
[111] Kim, J., and Kramer, T. A., 2006, "Improved Orthokinetic Coagulation Model for Fractal Colloids: Aggregation and Breakup," Chem. Eng. Sci., **61**, pp. 45–53.
[112] Wiltzius, P., 1987, "Hydrodynamic Behavior of Fractal Aggregates," Phys. Rev. Lett., **58**, pp. 710–713.
[113] Hess, W., Frisch, H. L., and Klein, R., 1986, "On the Hydrodynamic Behavior of Colloidal Aggregates," Z. Phys. B: Condens. Matter, **64**, pp. 65–67.
[114] Buongiorno, J., 2006, "Convective Transport in Nanofluids," ASME J. Heat Transfer, **128**, pp. 240–250.
[115] Goldhirsch, I., and Ronis, D., 1983, "Theory of Thermophoresis. I. General Considerations and Mode-Coupling Analysis," Phys. Rev. A, **27**, pp. 1616–1634.
[116] Lin, F., Bhatia, G. S., and Ford, J. D., 1993, "Thermal Conductivities of Powder-Filled Epoxy Resins," J. Appl. Polym. Sci., **49**, pp. 1901–1908.
[117] Boudenne, A., Ibos, L., Fois, M., Gehin, E., and Majeste, J.-C., 2004, "Thermophysical Properties of Polypropylene/Aluminum Composites," J. Polym. Sci., Part B: Polym. Phys., **42**, pp. 722–732.
[118] Tekce, H. S., Kumlutas, D., and Tavman, I. H., 2007, "Effect of Particle Shape on Thermal Conductivity of Copper Reinforced Polymer Composites," J. Reinf. Plast. Compos., **26**, pp. 113–121.
[119] Xu, Y., Chung, D. D. L., and Mroz, C., 2001, "Thermally Conducting Aluminum Nitride Polymer-Matrix Composites," Composites, Part A, **32**, pp. 1749–1757.
[120] Agari, Y., and Uno, T., 1986, "Estimation of Thermal Conductivities of Filled Polymers," J. Appl. Polym. Sci., **32**, pp. 5705–5712.
[121] Cowling, T. G., Gray, P., and Wright, P. G., 1963, "The Physical Significance of Formulae for the Thermal Conductivity and Viscosity of Gaseous Mixtures," Proc. R. Soc. London, Ser. A, **276**, pp. 69–82.
[122] Pandey, J. D., and Mishra, R. K., 2005, "Theoretical Evaluation of Thermal Conductivity and Diffusion Coefficient of Binary Liquid Mixtures," Phys. Chem. Liq., **43**, pp. 49–57.
[123] Assael, M. J., Charitidou, E., and Wakeham, W. A., 1989, "Absolute Measurements of the Thermal Conductivity of Mixtures of Alcohols With Water," Int. J. Thermophys., **10**, pp. 793–803.
[124] Li, C. C., 1976, "Thermal Conductivity of Liquid Mixtures," AIChE J., **22**, pp. 927–930.
[125] Li, Q., Xuan, Y., and Wang, J., 2005, "Experimental Investigations on Transport Properties of Magnetic Fluids," Exp. Therm. Fluid Sci., **30**, pp. 109–116.
[126] Jagannadham, K., and Wang, H., 2002, "Thermal Resistance of Interfaces in AlN-Diamond Thin Film Composites," J. Appl. Phys., **91**, pp. 1224–1235.
[127] Ge, Z., Cahill, D. G., and Braun, P. V., 2006, "Thermal Conductance of Hydrophilic and Hydrophobic Interfaces," Phys. Rev. Lett., **96**, p. 186101.
[128] Bryning, M. B., Milkie, D. E., Islam, M. F., Kikkawa, J. M., and Yodh, A. G., 2005, "Thermal Conductivity and Interfacial Resistance in Single-Wall Carbon Nanotube Epoxy Composites," Appl. Phys. Lett., **87**, p. 161909.
[129] Huxtable, S. T., Cahill, D. G., Shenogin, S., Xue, L., Ozisik, R., Barone, P., Usrey, M., Strano, M. S., Siddons, G., Shim, M., and Keblinski, P., 2003, "Interfacial Heat Flow in Carbon Nanotube Suspension," Nature Mater., **2**, pp. 731–734.
[130] Nan, C.-W., Liu, G., Lin, Y., and Li, M., 2004, "Interface Effect on Thermal Conductivity of Carbon Nanotube Composites," Appl. Phys. Lett., **85**, pp. 3549–3551.
[131] Wen, D., and Ding, Y., 2004, "Experimental Investigation Into Convective Heat Transfer of Nanofluids at the Entrance Region Under Laminar Flow Conditions," Int. J. Heat Mass Transfer, **47**, pp. 5181–5188.
[132] Wen, D., and Ding, Y., 2006, "Natural Convective Heat Transfer of Suspensions of Titanium Dioxide Nanoparticles (Nanofluids)," IEEE Trans. Nanotechnol., **5**, pp. 220–227.
[133] Shaikh, S., Lafdi, K., and Ponnappan, R., 2007, "Thermal Conductivity Improvement in Carbon Nanoparticle Doped PAO Oil: An Experimental Study," J. Appl. Phys., **101**, p. 064302.
[134] Choi, S. U. S., Zhang, Z. G., Yu, W., Lockwood, F. E., and Grulke, E. A., 2001, "Anomalous Thermal Conductivity Enhancement in Nanotube Suspensions," Appl. Phys. Lett., **79**, pp. 2252–2254.
[135] Hwang, Y., Lee, J. K., Lee, C. H., Jung, Y. M., Cheong, S. I., Lee, C. G., Ku, B. C., and Jang, S. P., 2007, "Stability and Thermal Conductivity Characteristics of Nanofluids," Thermochim. Acta, **455**, pp. 70–74.
[136] Wen, D., and Ding, Y., 2004, "Effective Thermal Conductivity of Aqueous Suspensions of Carbon Nanotubes (Carbon Nanotube Nanofluids)," J. Thermophys. Heat Transfer, **18**, pp. 481–485.
[137] Williams, W., Buongiorno, J., and Hu, L.-W., 2008, "Experimental Investigation of Turbulent Convective Heat Transfer and Pressure Loss of Alumina/Water and Zirconia/Water Nanoparticle Colloids (Nanofluids) in Horizontal Tubes," ASME J. Heat Transfer, **130**, p. 042412.
[138] Williams, W. C., 2006, "Experimental and Theoretical Investigations of Transport Phenomena in Nanoparticle Colloids (Nanofluids)," Ph.D. thesis, Department of Nuclear Science and Engineering, Massachusetts Institute of Technology, Cambridge, MA.
[139] Bertolini, D., and Tani, A., 1997, "Thermal Conductivity of Water: Molecular Dynamics and Generalized Hydrodynamics Results," Phys. Rev. E, **56**, pp. 4135–4151.
[140] Li, L., and Chung, D. D. L., 1994, "Thermally Conducting Polymer-Matrix Composites Containing Both AIN Particles and SIC Whiskers," J. Electron. Mater., **23**, pp. 557–564.
[141] National Institute of Standards and Technology (NIST), "Fluid Properties," http://webbook.nist.gov/chemistry/fluid/
[142] Rusconi, R., Williams, W., Buongiorno, J., Piazza, R., and Hu, L.-W., 2007, "Numerical Analysis of Convective Instabilities in a Transient Short-Hot-Wire Setup for Measurement of Liquid Thermal Conductivity," Int. J. Thermophys., **28**, pp. 1131–1146.
[143] 2007, "CRC Handbook of Chemistry and Physics," http://www.hbcpnetbase.com
[144] Kwak, K., and Kim, C., 2005, "Viscosity and Thermal Conductivity of Copper Oxide Nanofluid Dispersed in Ethylene Glycol," Korea-Aust. Rheol. J., **17**, pp. 35–40.
[145] "The A-Z of Materials," http://www.azom.com
[146] Weidenfeller, B., Höfer, M., and Schilling, F., 2002, "Thermal and Electrical Properties of Magnetite Filled Polymers," Composites, Part A, **33**, pp. 1041–1053.
[147] Bozorth, R. M., 1978, *Ferromagnetism*, IEEE, New York.
[148] Yu, R. C., Tea, N., Salamon, M. B., Lorents, D., and Malhotra, R., 1992, "Thermal Conductivity of Single Crystal C60," Phys. Rev. Lett., **68**, pp. 2050–2053.